Icarus 249 (2015) 22–42

Contents lists available at ScienceDirect

Icarus

journal homepage: www.elsevier.com/locate/icarus

Compositions of coarse and fine particles in martian soils at gale: A window into the production of soils

A. Cousin [a,*], P.Y. Meslin [b], R.C. Wiens [a], W. Rapin [b], N. Mangold [c], C. Fabre [d], O. Gasnault [b], O. Forni [b], R. Tokar [e], A. Ollila [f], S. Schröder [b], J. Lasue [b], S. Maurice [b], V. Sautter [g], H. Newsom [f], D. Vaniman [e], S. Le Mouélic [c], D. Dyar [h], G. Berger [b], D. Blaney [i], M. Nachon [c], G. Dromart [j], N. Lanza [a], B. Clark [k], S. Clegg [a], W. Goetz [l], J. Berger [m], B. Barraclough [e], D. Delapp [a], MSL Science Team

[a] Los Alamos National Laboratory, Los Alamos, NM 87544, USA
[b] Institut de Recherche en Astrophysique et Planétologie, Toulouse, France
[c] Laboratoire Planétologie et Géodynamique, LPGNantes, CNRS UMR 6112, Université de Nantes, France
[d] Université de Lorraine, Nancy, France
[e] Planetary Science Institute, Tucson, AZ 85719, USA
[f] University of New Mexico, Albuquerque, NM 87131, USA
[g] Museum National d'Histoire Naturelle, Paris, France
[h] Mount Holyoke College, South Hadley, MA 01075, USA
[i] Jet Propulsion Laboratory, California Institute of Technology, Pasadena, CA 91109, USA
[j] Laboratoire de Géologie de Lyon, France
[k] Space Science Institute, Bouler, CO 80301, USA
[l] Max Planck Institute for Solar System Research, Katlenburg-Lindau, Germany
[m] Department of Earth Sciences, Western University, London, ON N6A 5B7, Canada

ARTICLE INFO

Article history:
Received 6 November 2013
Revised 25 March 2014
Accepted 29 April 2014
Available online 9 May 2014

Keyword:
Mars
Mars, surface
Spectroscopy
Regoliths

ABSTRACT

The ChemCam instrument onboard the Curiosity rover provides for the first time an opportunity to study martian soils at a sub-millimeter resolution. In this work, we analyzed 24 soil targets probed by ChemCam during the first 250 sols on Mars. Using the depth profile capability of the ChemCam LIBS (Laser-Induced Breakdown Spectroscopy) technique, we found that 45% of the soils contained coarse grains (>500 μm). Three distinct clusters have been detected: Cluster 1 shows a low SiO_2 content; Cluster 2 corresponds to coarse grains with a felsic composition, whereas Cluster 3 presents a typical basaltic composition. Coarse grains from Cluster 2 have been mostly observed exposed in the vicinity of the landing site, whereas coarse grains from Clusters 1 and 3 have been detected mostly buried, and were found all along the rover traverse. The possible origin of these coarse grains was investigated. Felsic (Cluster 2) coarse grains have the same origin as the felsic rocks encountered near the landing site, whereas the origin of the coarse grains from Clusters 1 and 3 seems to be more global. Fine-grained soils (particle size < laser beam diameter which is between 300 and 500 μm) show a homogeneous composition all along the traverse, different from the composition of the rocks encountered at Gale. Although they contain a certain amount of hydrated amorphous component depleted in SiO_2, possibly present as a surface coating, their overall chemical homogeneity and their close-to-basaltic composition suggest limited, or isochemical alteration, and a limited interaction with liquid water. Fine particles and coarse grains from Cluster 1 have a similar composition, and the former could derive from weathering of the latter. Overall martian soils have a bulk composition between that of fine particles and coarse grains. This work shows that the ChemCam instrument provides a means to study the variability of soil composition at a scale not achievable by bulk chemical analyses.

* Corresponding author.
E-mail address: acousin@lanl.gov (A. Cousin).

http://dx.doi.org/10.1016/j.icarus.2014.04.052
0019-1035/

1. Introduction

Each *in situ* Mars mission has characterized the local soil composition, starting with Viking 1 and 2. The two Viking landers showed a similar composition at Chryse Planitia and Utopia Planitia, their respective locations (Toulmin et al., 1977; Baird et al., 1977; Clark et al., 1982). The martian surface was then studied by Mars Pathfinder at Ares Vallis (Rieder et al., 1997; Bell et al., 2000; Brückner et al., 2001; Wänke et al., 2001) and by the Mars Exploration Rovers (MER), with Spirit at Gusev Crater (Gellert et al., 2006) and Opportunity at Meridiani Planum (Rieder et al., 2004; Squyres et al., 2004; Yen et al., 2005). While there have been a few exceptions (e.g., Squyres et al., 2008) the analyses performed during these missions have shown a similar composition for the majority of the soil measurements in each of these locations. Moreover, they have shown that both bright dust and fine-grained, dark soil deposits show little chemical variation across the planet within measurement errors, reflecting either the existence of a global component or the general similarity in the compositions of the rocks from which they were derived (Yen et al., 2005). McGlynn et al. (2012) studied the relationship between the grain size and the composition of the soils at Gusev Crater and Meridiani Planum. They have estimated their modal mineralogy by using Mössbauer, MiniTES and APXS data. From these results, they showed that the fines were enriched in Fe and Mg compared to coarse grains, indicating that mafic phases were more abundant in fines than in coarse grains.

At a global scale, several mineralogical and elemental maps have been produced based on orbital imaging and spectroscopy that suggest more variability in the composition of the surficial materials. These have revealed regions that are distinct from each other in the thermal infrared (Bandfield et al., 2000), and in compositions derived from the Gamma Ray Spectrometer instrument on Mars Odyssey, with large-scale heterogeneities, corresponding to local and regional contributions to the material at the martian surface (Gasnault et al., 2010; Newsom et al., 2007). However, it is not clear from orbit if this represents a change in the surficial materials underlying the soil (to the depth of 0.5–1 m covered by GRS measurements) or whether these heterogeneities reflect only differences in the local bedrock composition. Heterogeneities observed by the GRS show that *in situ* missions do not cover the wide range of compositions on Mars.

Curiosity landed on August 6th, 2012 in Gale crater, Mars. With its 80 kg payload, this rover possesses unique analytical capabilities to investigate the chemistry and mineralogy of the martian soil (Grotzinger et al., 2012). In particular, the Laser-Induced Breakdown Spectroscopy (LIBS) technique is being used for the first time on another planet with the ChemCam instrument (Maurice et al., 2012a; Wiens et al., 2012). This is a remote-sensing technique (up to 7 m) which permits rapid analysis. It retrieves the chemical composition of soils and rocks with footprints between 350 and 550 μm, depending on the distance of the target (Maurice et al., 2012b). Moreover, it allows shallow (tens of μm to a few mm) chemical depth profile analysis, as it obtains a spectrum for each shot as repeated laser pulses probe progressively deeper into the target. Measurements are usually performed with 30 shots, but can be up to several hundred shots at each point location. Moreover, a series of 30 shots in a non-consolidated soil allows chemical analyses to depths of about 3.5–5 mm (Wiens et al., 2013). ChemCam has the highest resolution remote camera (the Remote Micro-Imager, or RMI) onboard *Curiosity* (Le Mouélic et al., 2015). Images are used to provide a geochemical context to the LIBS analyses, and locate the laser points on the targets.

Soil compositions from previous missions on Mars were acquired by the APXS instrument on Sojourner (Mars Pathfinder mission) and MER, and by the X-ray fluorescence instrument on Viking. The APXS footprint on MER was 3.8 cm diameter (Squyres et al., 2003), whereas on MSL it is 1.7 cm diameter (Gellert et al., 2009). ChemCam, with footprints ranging from 350 to 550 μm, is the first instrument on Mars able to sample soil particles at the sub-millimeter scale.

2. Geological settings

Within Gale crater, three regions have been visited during the first year of operations: Bradbury Rise, the Rocknest area, and the Yellowknife Bay area (Fig. 1). *Curiosity* landed at the Bradbury Rise, which corresponds to a distal portion of the alluvial fan from Peace Vallis (Palucis et al., submitted for publication). The area is dominated by regolith built from soils, pebbles, float rocks and local outcrops of conglomerates interpreted to be of fluvial origin (Sautter et al., 2013; Williams et al., 2013). Some of the pebbles and float rocks derive from the crater rim (Palucis et al., submitted for publication) whereas some may have been deposited ballistically (Newsom et al., 2014). The Rocknest area includes an aeolian bedform – a sand shadow scooped by the rover, and dark-toned rock outcrops and floats (Bish et al., 2013; Blake et al., 2013; Leshin et al., 2013; Meslin et al., 2013; Blaney et al., submitted for publication). The Yellowknife Bay area to the east of the two previous regions consists of outcrops of sediments interpreted as fluviolacustrine deposits (Grotzinger et al., submitted for publication). This area is characterized by three stratigraphic members: Sheepbed, Gillespie Lake and Glenelg (Grotzinger et al., submitted for publication). This region is characterized by in-place sedimentary mudstones and sandstones with almost no float rocks, in sharp contrast to Bradbury Rise.

ChemCam observed 189 targets along the 450 m the rover traversed from the Bradbury landing site during the first 250 sols, with 24 of these targets being soils (Fig. 2). The three regions mentioned above show only very limited soil horizon development. In the following, soil composition thus refers to the composition of loose and unconsolidated material that can be sufficiently small to be transported by wind or water. ChemCam provides a large number of separate analyses (the 24 targets represent 172 LIBS analysis points). These investigations are revealing for the first time heterogeneities in nearly all the soils encountered.

Based on initial ChemCam analyses from the first 90 sols, Meslin et al. (2013) have defined three kinds of soils, depending on their size and/or composition: (i) felsic soils, corresponding to coarse grains which are usually encountered at Bradbury, (ii) fine-grained mafic soils which are encountered throughout the rover traverse, and (iii) mixed soils with an intermediate composition. The coarsest component observed at the Bradbury site has a felsic composition, close to that of float rocks in the same area (Sautter et al., 2013): the latter study focused on ChemCam data acquired on five float rocks at Bradbury, revealing a magmatic diversity with feldspar-rich lithologies. On the other hand, the soils observed at Rocknest have a mafic composition, but distinct from the mafic rocks encountered elsewhere in Gale crater. Finally, the composition of the silt/fine sand particles measured by APXS and by ChemCam in an aeolian sand shadow at the Rocknest site in Gale crater was also found to be similar to the composition of the soils analyzed at other locations on Mars (Blake et al., 2013; Meslin et al., 2013).

At the RMI image scale (field of view of a few centimeters, spatial resolution around 2 pixels, and 1024 × 1024 pixels per image – Langevin et al., 2013), ChemCam analysis points are classified in this work into various types: 1. Coarse and fine grain mixtures; 2. Pebbles (4–64 mm); 3. Medium to coarse-grained sand (0.25–1 mm); 4. Fine-grained sand (<0.25 mm) (Table 1). Fig. 1 shows

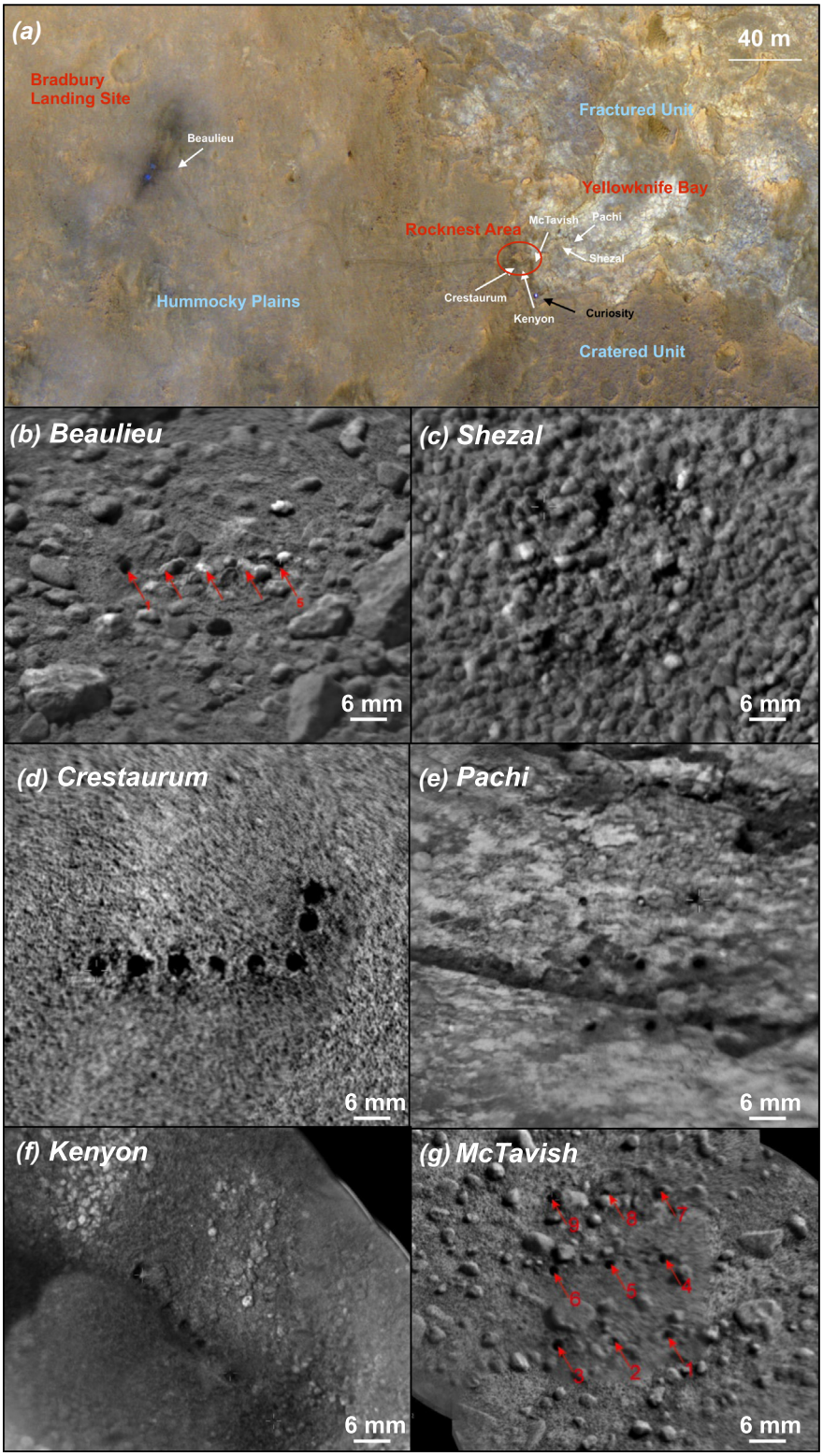

Fig. 1. Curiosity traverse up to sol 250 (24 soil targets) with some RMI examples of each type of soil analyzed by ChemCam. (A) Traverse up to sol 250 with location of these typical soils (image credit: NASA/JPL-Caltech/Univ. of Arizona), (B) Beaulieu corresponds to several types: point 1 (on the left) is considered as a fine-grained soil with a large laser crater. Point 5 (on the right) is considered as a mixing between cobble and soil, as it is impossible to discriminate between the two options. Points 2, 3 and 4 are exposed pebbles (covered by dust), (C) Shezal is considered as a coarse-grained soil, (D) Crestaurum is a fine-grained soil, (E) Pachi is a fine-grained compacted soil, due to its location in the rover wheels tracks, (F) Kenyon is a fine-grained soil from the scoop trench , and (G) McTavish is considered as a fine-grained soil, except the last 2 points, which are in the "cobble and soil" category. Image sources: (B) Mosaic from images "CR0_400422060EDR_F0040000CCAM04033M1" and "CR0_400422710EDR_F0040000CCAM04033M1", (C) mosaic from images "CR0_411859443EDR_F0051986CCAM02161M1" and "CR0_411860496EDR_F0051986CCAM02161M1", (D) mosaic from images "CR0_404935473EDR_F0050104CCAM03083M1" and "CR0_404936786EDR_F0050104CCAM03083M1", (E) mosaic from images "CR0_409475699EDR_F0051858CCAM03135M1" and "CR0_409476672EDR_F0051858CCAM03135M1", (F) mosaic from images "CR0_404758057EDR_F0050104CCAM01081M1", and "CR0_404759515EDR_F0050104CCAM01081M1", (G) mosaic from images "CR0_407883644EDR_F0050432CCAM01117M1" and "CR0_407884605EDR_F0050432CCAM01117M1".

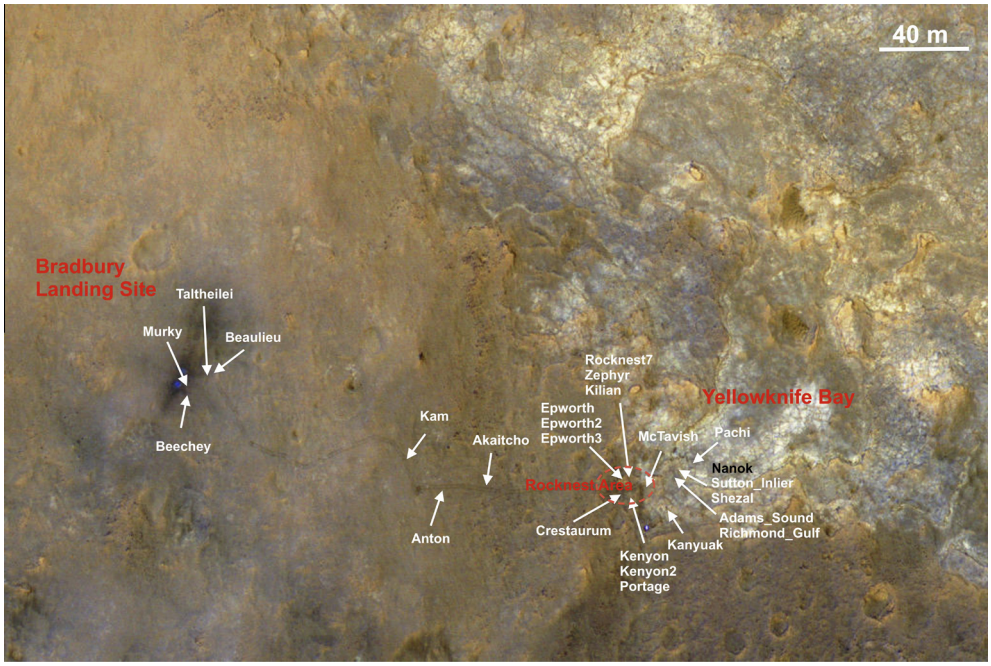

Fig. 2. Localization of the 24 soil targets (in white) sampled by ChemCam along the Curiosity traverse up to sol 250. Nanok, rock sampled at Yellowknife Bay is also shown (in black). In red are the three main geological units that Curiosity visited during the first 250 sols (image credit: NASA/JPL-Caltech/Univ. of Arizona). (For interpretation of the references to colour in this figure legend, the reader is referred to the web version of this article.)

Table 1
Particle sizes from the Wentworth scale (Wentworth, 1922). Particles smaller than Medium sand (included) are smaller than the laser beam, which is ~0.35 mm between 3.5 and 4 m in distance (Maurice et al., 2012b), which is the typical ChemCam range analysis at Gale, and are therefore part of what is called "fines" in this study.

Classification	Particle size (diameter)
Boulder	Above 256 mm
Cobble	64–256 mm
Pebble	4–64 mm
Gravel (or granule)	2–4 mm
Very coarse sand	1–2 mm
Coarse sand	0.5–1 mm
Medium sand	0.25–0.5 mm
Fine sand	0.125–0.25 mm
Very fine sand	0.062–0.125 mm
Silt	0.004–0.062 mm
Clay	Less than 0.004 mm

an image characteristic of each group, with "pebbles" corresponding to the pebbles (Table 1) encountered at the surface, and the type "coarse and fine-grain mixtures" meaning that from an RMI perspective, depending on the distance of the targets, it was difficult to know if a fine-grained soil or an exposed pebble or coarse grain were sampled, and analyses of the spectra were therefore required. Most of the analyzed soils correspond to undisturbed soils (66% of them). From an RMI point of view, 52% of the LIBS analysis points appeared fine-grained, while the distinction between fines and pebbles was difficult in 14% of the cases (Fig. 3). Due to the limited capability of characterizing the size of buried material with RMI images, we implemented another technique to detect the presence of coarse grains in the soil, as described below.

This study is focused on the geochemical diversity that is observed between different soil separates, in particular between fine and coarse soils, whose mobility and geographical origin are likely to be different. We consider as "coarse grains" all particles from coarse sand up to pebbles in terms of size (these particles have a diameter equal to or larger than the laser beam diameter). We consider fine-grained particles (hereafter referred to as "fines") those having diameters smaller than the laser beam, and therefore corresponding to medium sand, silt and clay size fractions (Table 1).

3. Techniques and methods

All the data used in this study are obtained by the ChemCam instrument, which uses the LIBS technique. This part of the paper will describe this technique and then define all the qualitative and quantitative tools used to analyze the data. Then we will present the methodology developed to detect buried coarse grains in the soil.

3.1. LIBS technique

The ChemCam instrument (Maurice et al., 2012a; Wiens et al., 2012) is composed of two parts: one located on the mast of the rover, which contains the send and receive optics (laser, camera, telescope) and one located in the rover body (spectrometers). The LIBS technique consists of focusing a pulsed laser (1067 nm) onto a small area of the analyzed sample (350–550 μm). The laser/matter interaction ablates a small amount of the sample (a few ng) and creates a plasma. The plasma light emission is then collected by the telescope and passed to the spectrometers. ChemCam contains three spectrometers, from the ultraviolet (240 nm) up to the near-infrared (~900 nm). Each spectrum (from ultraviolet to near-infrared) consists of 6144 channels. Each element is characterized by various emission lines all along this range. A dedicated ChemCam library has been created under martian atmospheric pressure (Cousin et al., 2011).

ChemCam observations usually involve several point analyses on the same target, with at least 30 laser pulses (shots) per location. As a spectrum is acquired for each shot, we collect at least 30 spectra per location. This technique is useful for depth profile analyses.

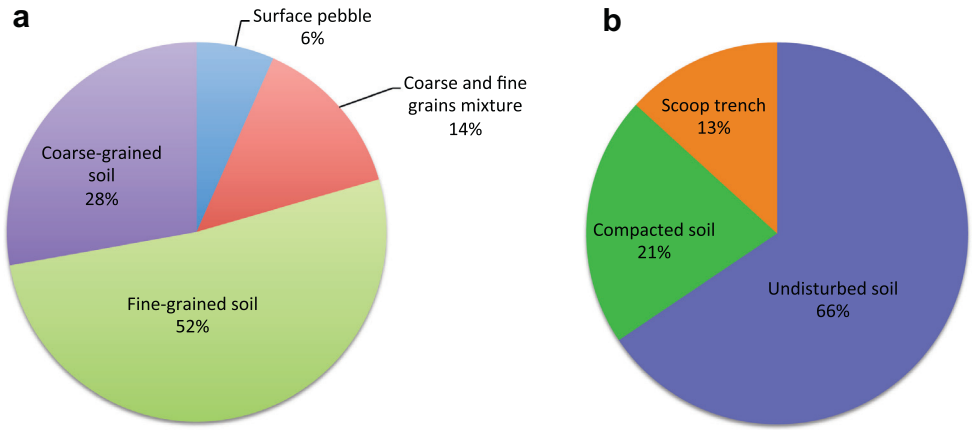

Fig. 3. Soil classification from RMI observations: (a) classification based on grain size only, (b) distribution of disturbed and un-disturbed soils among ChemCam analyses.

The acquired spectra are systematically corrected before they are used for quantitative or qualitative analyses. They are calibrated in wavelength, noise-corrected, and the background and continuum are removed (Wiens et al., 2013).

ChemCam can detect a range of elements, depending on their concentration: all the major (Si, Ca, Mg, Al, K, Na, Ti, and Fe), some minor and trace elements (H, C, N, P, S, Cl, Mn, Li, B, Rb, Sr, Ba, Cr, Ni, Cu, Zn, As, Cd, and Pb) with different detection limits (Maurice et al., 2012a,b). Moreover, ChemCam also contains a remote camera called RMI, which is useful to understand the context of the analyses. More information about the RMI and image products can be found in (Le Mouélic et al., 2015).

3.2. Qualitative and quantitative tools

The qualitative tools used in this study are aimed at discriminating the data and better visualizing them.

Independent component analysis (ICA) is a multivariate technique, a useful tool to perform a classification of ChemCam data (Forni et al., 2009, 2013; Lasue et al., 2011). This technique derives from blind source separation research (Hyvärinen et al., 2001), and identifies different statistically independent components allowing spectra to be sorted depending on these components, which are directly related to chemical elements (see SOM). Once the components are obtained, covariance scores are computed for each component. ICA is used here as a qualitative tool, although the scores are related to the abundances, but not in a simple linear relationship. This technique is very efficient to observe trends in a data set, and to classify the spectra.

The Sammon's map technique is a multidimensional scaling transformation that maps a high-dimensional data set to a lower number of dimensions in order to facilitate its visualization (Sammon, 1969; Lasue et al., 2011). The technique finds the optimal representation of the data, and is very useful for a 2-D classification of ChemCam data (Lasue et al., 2011). However, even if the projection makes it easier to visualize the relationship between data points and clustering, the non-linearity of the projection decorrelates the directions of the projection space and compositional trends in the data set, in contrast to ICA where the axis correspond to a single element.

A clustering technique called "K-means clustering" (Duda and Hart (1973), Seber (1984)) was also used in order to classify the spectra in groups, depending on their similarities. This technique has been shown to classify ChemCam LIBS spectra into physically reasonable and chemically distinct groups (Tokar et al., 2013). For an input number of clusters, the process is initialized by randomly assigning ChemCam spectra to a cluster. The algorithm moves spectra between clusters until the total sum of the squared Euclidean distance of each spectrum from the average spectra of its cluster is minimized.

To retrieve elemental compositions from processed spectra, two techniques are used: univariate analysis and a partial least squares technique (PLS). Univariate analysis correlates the LIBS signal for each element with a known emission line using calibration standards, which leads to a calibration curve (Fabre et al., in press). Several methods exist for preprocessing the signal before analysis, such as using the signal normalized by the total intensity, or using an internal standard (Sallé et al., 2006). The calibration standards are the calibration targets located on the rover (Fabre et al., 2011; Vaniman et al., 2012).

The PLS technique is a multivariate analysis method which is commonly used for LIBS (Clegg et al., 2009; Tukker et al., 2010; more information in the SOM). It reduces the number of variables to a few components while taking into account the whole spectral range (Martens and Naes, 1989). For those analyses, a standard database was created from pre-flight spectra from the ChemCam Flight Model with samples under martian and ambient conditions (Wiens et al., 2013). PLS regresses the spectral training set of standards of known composition, using principal components to fit the unknown samples and determine their compositions. For this study, we used a variant of PLS called PLS1, where a separate model was computed and optimized for each of the major element oxides (instead of using only one model for all oxides). More details can be found in supplementary material.

The accuracy of both methods is estimated by taking the root mean square error of prediction (RMSEP) from a leave-one-out cross-validation procedure on the training set. The RMSEPs for PLS analyses are: ±7.1 wt% for SiO_2, ±0.55 for TiO_2, ±3.7 for Al_2O_3, ±4.0 for FeO, ±3.0 for MgO and CaO, ±0.7 for Na_2O, and ±0.9 for K_2O. Each number of components was chosen by selecting the lowest RMSEP obtained on cross calibration, and using the calibration targets on Mars, both within one standard error of the minimum value. For both techniques, quantification of chemical analysis from LIBS data remains challenging due to overlapping elemental lines, dependence on the database that is used for the model, representativeness of this database, matrix effects (Chaléard et al., 1997; Panne et al., 1998; Aragon et al., 1999; Cremers and Radziemski, 2006) and distance effects (Melikechi et al., in press). In this paper, we used the PLS1 technique for quantification, which in the end was giving the same results as univariate analysis, within their respective error bars.

3.3. Methodology for detecting buried coarse grains

Most of the time, coarse grains can be seen in RMI images. However, we suspect than some of them are buried in the soil or covered by dust. With the ChemCam LIBS data, the following techniques can be used to identify a coarse grain: (i) variation of the total LIBS emission intensity summed over all channels, and (ii) comparison of shot-to-shot elemental composition variations.

When carried out on a rock surface, a sequence of LIBS shots generates spectra for which the sum of intensities in all spectral channels shows very little shot-to-shot variability (<10%) after the first few shots corresponding to a dust cover (Fig. 4a). By contrast, soils show a high variability in intensity when no buried coarse grain is encountered (Fig. 4b). This difference is not fully understood yet: this could be due to the difference of cohesion between a consolidated sample and a loose soil, which is more strongly disturbed by the laser shots, but it could also be due a component in the soil that could quench the plasma and therefore alter the signal (such as H for example). Whatever the reason, each rock acquired so far has shown a high stability in the signal, in contrast to loose soils.

From these observations we assumed that within a soil a subset of shots with low variability could reveal a coarse grain, called a grain candidate, which is hit several times before it has been moved or destroyed by the laser shock wave from the expanding plasma. While the beam is hitting the coarse grain the intensity and composition are stable, or vary smoothly. This was confirmed for LIBS points that were clearly targeted on exposed pebbles as seen in RMI images. Patterns of intensity and composition were studied carefully in the shot-to-shot data from several targets which were obvious examples (like Akaitcho #7). Following this, we used an automated process to generate a list of grain candidates from soil data. Detection of a coarse-grain candidate occurs within a subset of shots selected within the series that comprises the overall observation at a given location. We use the standard deviation of the derivative of the total intensity normalized to the average as a measure of variability. It is no higher than 0.06 for 90% of shot sequences on rocks and no higher than 0.25 for all the soils. Hence, the algorithm gives shot-to-shot intensity profiles for all subsets at each location interrogated down to as few as four shots: for each subset with variability lower than 0.06 a score is generated. The score is equal to the variability divided by the size of the subset that is squared in order to favor large subsets. Following this process, the subset with the lowest score is marked as a coarse grain candidate.

We have also used ICA to investigate the presence of coarse grains in the soils. A study using the signal stability technique presented above (Meslin et al., 2013) suggested that the coarse grains encountered from Bradbury to Rocknest have a composition that is statistically distinct from the fines, but this trend may not be systematic everywhere. We used the scores obtained for the Na component versus the scores obtained for the H component (Fig. 5). The Na scores are useful to discriminate between felsic and non-felsic coarse grains, whereas the H scores help to distinguish the dust and/or the fines (except if the coarse grain is hydrated). In a fine-grained soil, single-shot spectra are dispersed (Fig. 5a). In a fine-grained soil containing a buried lithic fragment, data form two clusters with distinct dispersions (Fig. 5b). In this specific example, the coarse grain exhibits a higher Na component and a lower H component.

Coarse grains observed at the surface vary in size from 0.5 mm up to 6 mm or larger (based on RMI observations), corresponding on the Wentworth scale to coarse sand [from 0.5 to 1 mm], up to pebbles [from 4 to 64 mm] (Table 1). For example, pebbles were visually observed at targets McTavish and Beaulieu (sols 117 and 33), gravels were observed at Kam (sol 43) and very coarse sand at Akaitcho and at Rocknest7 (sols 50 and 59). It is much more difficult to determine the size of coarse grains that are buried. Their extent in terms of number of shots was found to vary between 5 and 85 shots (out of a maximum of 100 shots in a single point location). Nevertheless, most of the time ChemCam is still sampling the coarse grain during the last shot, so this means than the grain could be much bigger, and could be a gravel, pebble or even a buried rock or lithic fragment. Moreover, the coarse grains must be bigger than the beam diameter (350–550 μm; Maurice et al., 2012b) to be sampled individually.

The detection of coarse grains, gravels and pebbles in the soil is therefore useful to study the relationship between chemical and physical properties of soil constituents and finally to focus on the fine-grained particles, hereafter referred to as "fines". In a point analysis, they are defined as the material sampled by all the laser shots that do not correspond to a buried coarse grain. They most likely correspond to particles <500 μm, because they should be smaller than the size of the laser beam, and because the martian soil seems largely devoid of coarse sand grains (0.5–1 mm) (Goetz et al., 2010; Pike et al., 2011). They cover all size fractions from clays to medium sand grains (Table 1), including airborne dust that is probably mixed in the soil. Shot-to-shot observations have shown that at least the first two shots are systematically different from the substratum for each kind of target, and thus most likely correspond to pure, or almost pure dust particles. However, these first two shots were excluded from the present analysis of "fine particles", as they will be more specifically addressed in a future study. Moreover, in order to avoid any LIBS transition effects between fines and coarse grains, we did not consider the two shots of the fines closest to the coarse grain. Therefore in the example of

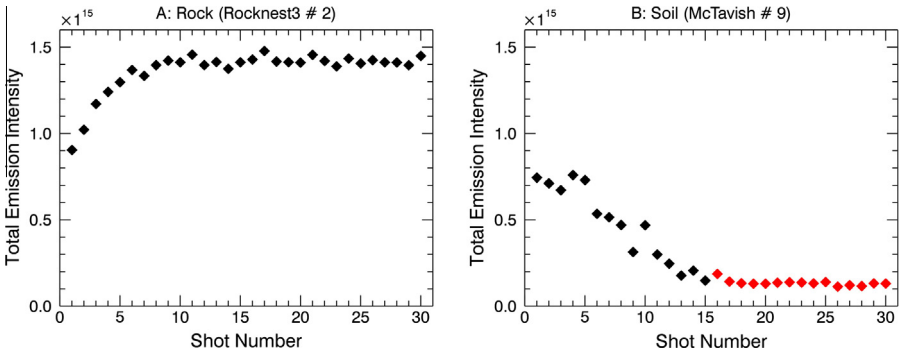

Fig. 4. Variation of the total emission intensity with shot number (30 shots on each point) on (A) a rock (Rocknest3 point #2), where the variability is lower than 10%, (B) a soil (Mc Tavish, point #9). This soil shows a high variability in intensity up to shot 15. Then, the variability is lower than 15% (red points) and this is attributed to the presence of a coarse grain from shot 15 to shot 30. (For interpretation of the references to colour in this figure legend, the reader is referred to the web version of this article.)

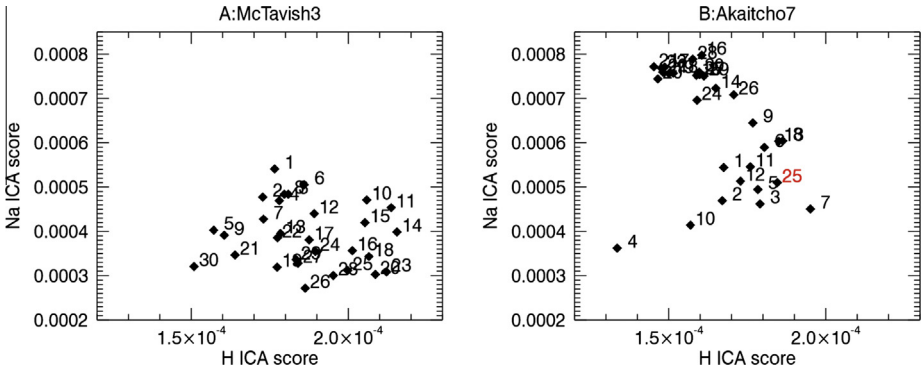

Fig. 5. Na ICA scores versus H ICA scores obtained for a shot by shot analysis. (A) Scores obtained for a fine-grained soil with no buried coarse grain (target called "Mc Tavish", point 3). (B) Scores obtained for a fine-grained soil with a buried coarse grain (target called "Akaitcho", point 7). Because ICA scores are a qualitative way of representing data, the axes do not correspond to direct abundances. One cluster is observed with a higher variance for the Na component and a lower variance for the H component. This main cluster is interpreted as a signature of a buried coarse grain. Points outside this cluster thus correspond to shots having sampled fine particles. We can observe for the Akaitcho target that shot 25 is not part of the cluster, as its Na score is lower whereas it shows a higher H score than the other final 10 points. Thus, shot 25 may reflect dust particles that fell back into the crater.

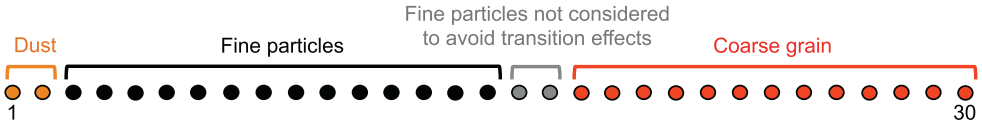

Fig. 6. Schematic representation of a 30-shot analysis point, illustrating which shots usually correspond to dust and which shots are discarded at the interface between fine particles and a coarse grain. In this case the coarse grain is sampled by the last 13 shots.

Fig. 6, we consider the fines only from shots 3 to 16. We take an additional precaution to avoid single shots that would lie in between surface dust and a coarse grain just beneath it. This unique shot could indeed represent a chemical transition between surficial dust and the grain.

4. Results

4.1. Compositions of the coarse grains

Using the two methods of total-intensity variation and ICA component covariance on the 24 soil targets (therefore 172 point analysis) we found that 45% of those soils contain at least one coarse grain, either at the surface or buried (Table 2). Among those clasts, 86% are buried, invisible in RMI images. Several techniques have been used to investigate those grains. First, a clustering tool was used in order to classify each spectrum. Then, the ICA technique was used to determine elemental composition relationships between each cluster. The results were compared using a Sammon's map.

The clustering tool allowed us to classify the 77 coarse-grain spectra into three groups. This technique clusters the data depending on their similarities. In order to understand the relationship between each group, we used the ICA technique. Fig. 7a shows an ICA result where the three clusters (distinguished by a color-code) are discriminated by their covariance with the Na and Si components. Cluster 2 has a higher covariance with the Na and Si components, whereas Cluster 1 seems to be poorly correlated (low covariance) with these components. Cluster 3 is intermediate between these two groups. Fig. 7b represents a Sammon's map plot obtained for these three groups. In this case Cluster 3 is clearly discriminated. Spectral analysis confirms that Cluster 2 is enriched in Na, Si, Ca and Al (in red in Fig. 7c), whereas Cluster 1 is enriched in H, and is poorer in Na, Al, Si and Ca (in blue in Fig. 7c) compared to Clusters 2 and 3. Cluster 3 (in green in Fig. 7c) displays more Fe, Ti, Ca, Al, Na, Cr and Mn contribution and less H than Cluster 1. This third group is a chemically distinct one and is not a mixture of Clusters 1 and 2. The Cr content in Cluster 3 is correlated with the MgO content, but not with the Al content, which suggests that it is associated with pyroxene phases, like Ti-rich augite, and not with spinel. The ICA observations agree with the compositions determined from the spectra and with the clustering results, and reflect those made by Meslin et al. (2013) in the soils. Cluster 3 is the most frequently sampled, corresponding to 52% of all the coarse grains. Cluster 2 corresponds to 29% of all the coarse grains, and Cluster 1 is the less populated, corresponding to 19% of the whole population of coarse grains detected.

Coarse grain compositions (in oxides, wt%) have been determined using the PLS1 technique. The quantitative values acquired for these coarse grains are reported as molar ratios in Fig. 8. Precision is shown has the standard deviation obtained from the Shergottite calibration target, present on the rover (Fabre et al., 2011). The data show a typical basaltic mixing line between felsic and mafic minerals. Cluster 2 is close to the felsic end (Albite/Orthoclase). Cluster 3 is plotted along the mixing line between the other two groups. Clusters 1 and 3 show some overlap close to the mafic end, because some of the Cluster 3 coarse grains display more Fe than others.

Some coarse grains are more hydrated, as they show a higher covariance with the H component. Most of them are part of Cluster 1 (McTavish 5, RichmondGulf 3, Kenyon 6 and Shezal 7), but some are part of Cluster 3 (Anton 4, Epworth2_1). All of them are buried grains encountered in a fine-grained soil, or in a compacted soil. All these points show some diversity in composition, and several hypotheses are possible: these coarse grains could be hydrated minerals, or also hydrated glass. Those coarse grains could also correspond to aggregates of fine particles or could also be the result of fine particles recrystallization (see part 4.1). This observation is still therefore not well understood.

Coarse grains in Cluster 1 show a very low major element total, close to 73% (whereas it is between 90% and 100% for the other groups of coarse grains). This group has a composition similar to that of mafic minerals, but could also contain material like glass or alteration phases with similar bulk composition.

Table 2
List of the 24 soil targets (with sol and sequence number) analyzed by ChemCam during the first 250 sols. The presence of a coarse grain with its group number is indicated.

Sol number	Sequence	Soil target name	Presence of coarse grain	Group of coarse grain
19	ccam03019	Beechey point 1	Yes	Cluster 3
19	ccam03019	Beechey point 2	Yes	Cluster 2
19	ccam03019	Beechey point 3	Yes	Cluster 1
19	ccam03019	Beechey point 4		
19	ccam03019	Beechey point 5	Yes	Cluster 2
22	ccam03022	Murky point 1	Yes	Cluster 3
22	ccam03022	Murky point 2	Yes	Cluster 2
22	ccam03022	Murky point 3	Yes	Cluster 3
22	ccam03022	Murky point 4	Yes	Cluster 2
22	ccam03022	Murky point 5		
32	ccam03032	Taltheilei point 1		
32	ccam03032	Taltheilei point 2		
32	ccam03032	Taltheilei point 3		
32	ccam03032	Taltheilei point 4		
32	ccam03032	Taltheilei point 5		
33	ccam04033	Beaulieu point 1		
33	ccam04033	Beaulieu point 2	Yes	Cluster 2
33	ccam04033	Beaulieu point 3	Yes	Cluster 2
33	ccam04033	Beaulieu point 4	Yes	Cluster 2
33	ccam04033	Beaulieu point 5	Yes	Cluster 3
43	ccam03043	Kam point 1	Yes	Cluster 2
43	ccam03043	Kam point 2		
43	ccam03043	Kam point 3		
43	ccam03043	Kam point 4	Yes	Cluster 3
43	ccam03043	Kam point 5	Yes	Cluster 2
43	ccam03043	Kam point 6	Yes	Cluster 2
43	ccam03043	Kam point 7	Yes	Cluster 2
43	ccam03043	Kam point 8		
43	ccam03043	Kam point 9	Yes	Cluster 2
49	ccam02049	Anton point 1	Yes	Cluster 3
49	ccam02049	Anton point 2	Yes	Cluster 3
49	ccam02049	Anton point 3	Yes	Cluster 3
49	ccam02049	Anton point 4	Yes	Cluster 3
49	ccam02049	Anton point 5	Yes	Cluster 2
50	ccam01050	Akaitcho point 1	Yes	Cluster 1
50	ccam01050	Akaitcho point 2		
50	ccam01050	Akaitcho point 3		
50	ccam01050	Akaitcho point 4		
50	ccam01050	Akaitcho point 5		
50	ccam01050	Akaitcho point 6		
50	ccam01050	Akaitcho point 7	Yes	Cluster 3
50	ccam01050	Akaitcho point 8		
50	ccam01050	Akaitcho point 9	Yes	Cluster 3
59	ccam01059	Rocknest7 point 1		
59	ccam01059	Rocknest7 point 2		
59	ccam01059	Rocknest7 point 3	Yes	Cluster 3
59	ccam01059	Rocknest7 point 4		
59	ccam01059	Rocknest7 point 5	Yes	Cluster 3
71	ccam02071	Zephyr point 7		
71	ccam02071	Zephyr point 8		
71	ccam02071	Zephyr point 9		
72	ccam02072	Epworth point 1	Yes	Cluster 3
72	ccam02072	Epworth point 2		
72	ccam02072	Epworth point 3	Yes	Cluster 3
72	ccam02072	Epworth point 4	Yes	Cluster 3
72	ccam02072	Epworth point 5	Yes	Cluster 3
72	ccam03072	Kilian point 5		
74	ccam01074	Crestaurum point 1		
74	ccam05074	Crestaurum point 2		
79	ccam01079	Epworth2 point 1	Yes	Cluster 3
79	ccam01079	Epworth2 point 2		
79	ccam01079	Epworth2 point 3	Yes	Cluster 3
79	ccam01079	Epworth2 point 4		
79	ccam01079	Epworth2 point 5		
79	ccam01079	Epworth2 point 6		
79	ccam01079	Epworth2 point 7		
79	ccam01079	Epworth2 point 8		
79	ccam01079	Epworth2 point 9	Yes	Cluster 1
79	ccam01079	Epworth2 point 10		
81	ccam01081	Kenyon point 1		
81	ccam01081	Kenyon point 2		
81	ccam01081	Kenyon point 3		
81	ccam01081	Kenyon point 4		
81	ccam01081	Kenyon point 5	Yes	Cluster 3

(*continued on next page*)

Table 2 (*continued*)

Sol number	Sequence	Soil target name	Presence of coarse grain	Group of coarse grain
81	ccam01081	Kenyon point 6	Yes	Cluster 1
81	ccam01081	Kenyon point 7		
81	ccam01081	Kenyon point 8	Yes	Cluster 2
81	ccam01081	Kenyon point 9		
81	ccam01081	Kenyon point 10		
84	ccam02084	Epworth3 point 1		
84	ccam02084	Epworth3 point 2	Yes	Cluster 3
84	ccam02084	Epworth3 point 3	Yes	Cluster 1
84	ccam02084	Epworth3 point 4		
84	ccam02084	Epworth3 point 5		
84	ccam02084	Epworth3 point 6		
84	ccam02084	Epworth3 point 7		
84	ccam02084	Epworth3 point 8		
84	ccam02084	Epworth3 point 9		
84	ccam02084	Epworth3 point 10		
84	ccam02084	Epworth3 point 11		
84	ccam02084	Epworth3 point 12		
84	ccam02084	Epworth3 point 13		
84	ccam02084	Epworth3 point 14		
84	ccam02084	Epworth3 point 15	Yes	Cluster 3
89	ccam02089	Portage point 1		
89	ccam02089	Portage point 2	Yes	Cluster 1
89	ccam02089	Portage point 3		
89	ccam02089	Portage point 4	Yes	Cluster 3
89	ccam02089	Portage point 5		
89	ccam02089	Portage point 6		
89	ccam02089	Portage point 7		
89	ccam02089	Portage point 8	Yes	Cluster 3
89	ccam02089	Portage point 9		
97	ccam02097	Kenyon2 point 1		
97	ccam02097	Kenyon2 point 2		
97	ccam02097	Kenyon2 point 3		
97	ccam02097	Kenyon2 point 4	Yes	Cluster 3
97	ccam02097	Kenyon2 point 5	Yes	Cluster 3
97	ccam02097	Kenyon2 point 6		
97	ccam02097	Kenyon2 point 7	Yes	Cluster 1
97	ccam02097	Kenyon2 point 8		
97	ccam02097	Kenyon2 point 9		
97	ccam02097	Kenyon2 point 10		
117	ccam01117	McTavish point 1	Yes	Cluster 3
117	ccam01117	McTavish point 2	Yes	Cluster 2
117	ccam01117	McTavish point 3		
117	ccam01117	McTavish point 4		
117	ccam01117	McTavish point 5	Yes	Cluster 1
117	ccam01117	McTavish point 6		
117	ccam01117	McTavish point 7	Yes	Cluster 3
117	ccam01117	McTavish point 8	Yes	Cluster 3
117	ccam01117	McTavish point 9	Yes	Cluster 2
123	ccam01123	Kanyuak point 1	Yes	Cluster 2
123	ccam01123	Kanyuak point 2		
123	ccam01123	Kanyuak point 3	Yes	Cluster 2
123	ccam01123	Kanyuak point 4	Yes	Cluster 1
123	ccam01123	Kanyuak point 5	Yes	Cluster 2
123	ccam01123	Kanyuak point 6		
123	ccam01123	Kanyuak point 7		
123	ccam01123	Kanyuak point 8	Yes	Cluster 1
123	ccam01123	Kanyuak point 9		
135	ccam03135	Pachi point 1	Yes	Cluster 1
135	ccam03135	Pachi point 2		
135	ccam03135	Pachi point 3	Yes	Cluster 1
135	ccam03135	Pachi point 4		
135	ccam03135	Pachi point 5		
135	ccam03135	Pachi point 6		
135	ccam03135	Pachi point 7	Yes	Cluster 2
135	ccam03135	Pachi point 8	Yes	Cluster 2
135	ccam03135	Pachi point 9	Yes	Cluster 2
161	ccam02161	Shezal point 1	Yes	Cluster 3
161	ccam02161	Shezal point 2		
161	ccam02161	Shezal point 3	Yes	Cluster 3
161	ccam02161	Shezal point 4	Yes	Cluster 1
161	ccam02161	Shezal point 5	Yes	Cluster 3
161	ccam02161	Shezal point 6		
161	ccam02161	Shezal point 7	Yes	Cluster 1
161	ccam02161	Shezal point 8		
161	ccam02161	Shezal point 9		

Table 2 (*continued*)

Sol number	Sequence	Soil target name	Presence of coarse grain	Group of coarse grain
169	ccam03169	Sutton_Inlier point 1	Yes	Cluster 3
169	ccam03169	Sutton_Inlier point 2		
169	ccam03169	Sutton_Inlier point 3		
169	ccam03169	Sutton_Inlier point 4	Yes	Cluster 3
174	ccam01174	Sutton_Inlier2 point 1		
174	ccam01174	Sutton_Inlier2 point 2		
174	ccam01174	Sutton_Inlier2 point 3		
174	ccam01174	Sutton_Inlier2 point 4		
193	ccam02193	Adams_Sound point 1		
193	ccam02193	Adams_Sound point 2		
193	ccam02193	Adams_Sound point 3	Yes	Cluster 3
193	ccam02193	Adams_Sound point 4	Yes	Cluster 3
193	ccam02193	Adams_Sound point 5		
193	ccam02193	Adams_Sound point 6	Yes	Cluster 3
193	ccam02193	Adams_Sound point 7		
193	ccam02193	Adams_Sound point 8	Yes	Cluster 3
193	ccam02193	Adams_Sound point 9	Yes	Cluster 3
193	ccam02193	Adams_Sound point 10	Yes	Cluster 3
194	ccam01194	Richmond_Gulf point 1		
194	ccam01194	Richmond_Gulf point 2		
194	ccam01194	Richmond_Gulf point 3	Yes	Cluster 1
194	ccam01194	Richmond_Gulf point 4		
194	ccam01194	Richmond_Gulf point 5		

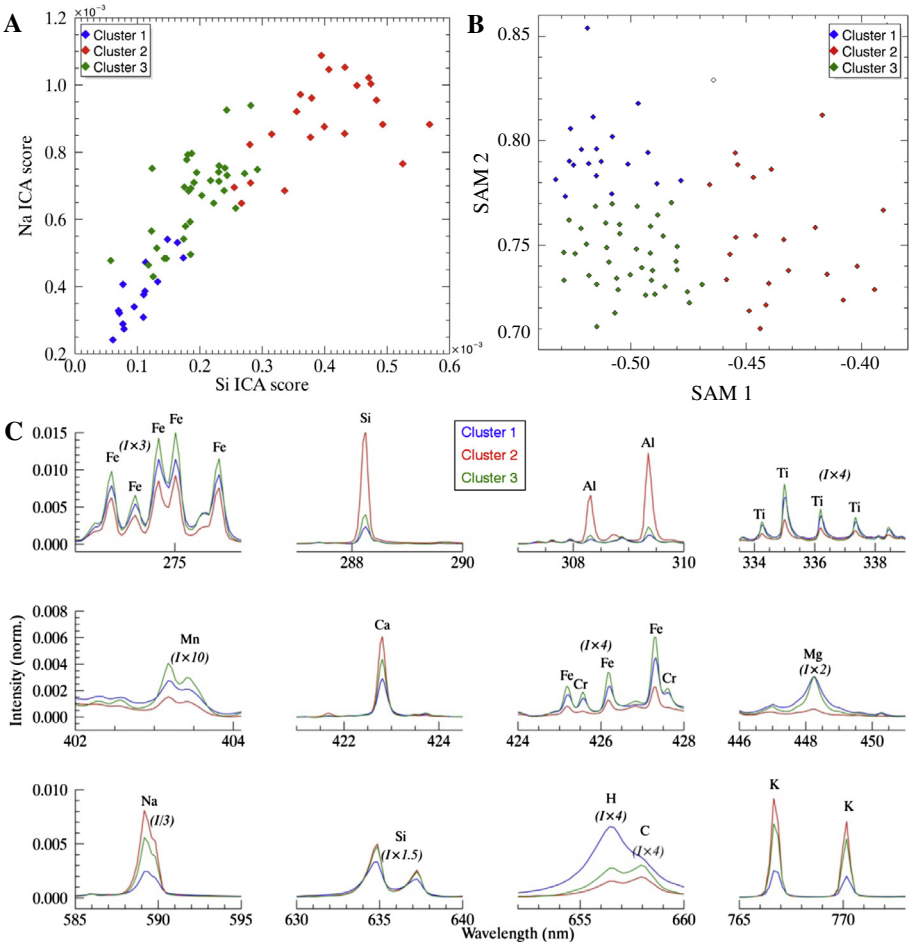

Fig. 7. (A) ICA plot representing the ICA scores obtained for the Na component versus the ICA scores obtained for the Si component for each coarse grain. Each cluster obtained by the clustering tool is represented by a different color. Scores obtained for Cluster 2 are always higher for the Na and Si components, whereas Cluster 1 scores are the lowest for these two components. (B) Sammon's map representation for each cluster. This representation allows identification of three clusters, consistent with those defined from the clustering analysis. The white point is Epworth 5, the Ca-rich target removed from this study. (C) Close-up of several spectral regions for each of the three clusters. The spectral ranges of interest show the main spectral differences between the three groups of coarse grains. (For interpretation of the references to colour in this figure legend, the reader is referred to the web version of this article.)

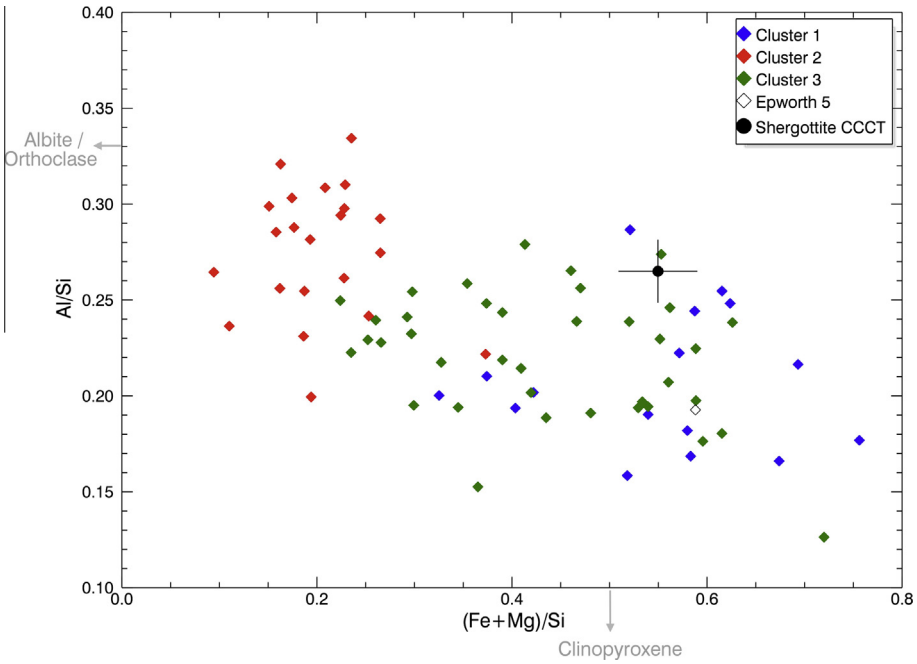

Fig. 8. Al/Si versus (Fe + Mg)/Si diagram of all the coarse grains (molar ratios). A mixing line is observed between the albite and the clinopyroxene/olivine endmembers (olivine is located at 2.0 on the *x*-axis). The average accuracy is 0.11 on the *y*-axis and 0.21 on the *x*-axis. The average value with its standard deviation obtained for all the Shergottite calibration target (Fabre et al., 2011) analyses observed at 40 Amps is over-plotted in order to give the precision obtained by ChemCam on solid samples.

One coarse grain is the richest soil target in Ca ever analyzed to date by ChemCam (around 28 wt% of CaO) and was encountered at Epworth point 5 on top of the Rocknest sand shadow. This coarse grain is also rich in fluorite and fluor-apatite (Forni et al., 2014), and will not be taken into account for this study as it is an outlier and is discussed in other studies (Forni et al., submitted for publication). Its presence in the soil, however, results from the weathering of local rocks.

4.2. Composition of the fines

4.2.1. Are the fines homogeneous?

Fig. 9 shows all the shots corresponding to the fines using molar elemental ratios determined by PLS1 technique. The fines display primarily a single cluster of typical basaltic composition centered between the plagioclase and mafic end-members. They show a composition consistent with the CheMin analysis (Bish et al., 2013). This CheMin analysis was performed on fine-grained soil fractions (<150 μm) at the Rocknest aeolian bedform in Gale (Fig. 1), using the X-ray diffraction technique. They revealed the presence of plagioclase, olivine enriched in Mg, augite and pigeonite, with some alkali feldspars, and some Fe-oxides. Nevertheless, plagioclase analyzed by CheMin were less enriched in Na than those analyzed by ChemCam in coarse grains (labradorite versus albite, respectively).

The dispersion of the data shown in Fig. 9 probably results from several effects: first, it reflects some level of chemical heterogeneity within the fine-grained particles. This is not unexpected given the variability in mineralogy observed by CheMin, and the variability in grain morphologies and colors observed on MAHLI images (e.g., Fig. 14) and on microscopic images of the martian soil made at the Phoenix landing site (Goetz et al., 2010). However, some dispersion probably also reflects the larger variability in the laser-target coupling characterizing unconsolidated materials, which could result in a larger variability of the chemical compositions inferred by the PLS technique, although the spectra are normalized by their total intensities. The contribution of the latter effect will be assessed by laboratory experiments. Meanwhile, we can estimate an upper and a lower limit of the precision of the chemical data shown in Fig. 9. The standard deviation of the data shown in this figure represents an upper limit, and the standard deviation obtained on one of the onboard calibration target (Shergottite) with similar composition (shown in Fig. 8) a lower limit.

Some shots are closer to the albite/orthoclase composition and significantly different from the mean composition, revealing some heterogeneity within the fines. The fines with a more felsic composition correspond to some targets encountered at Rocknest (Kenyon 8 and 10, Pachi 7) and Yellowknife Bay (Kanyuak 1). Kenyon 8 and Pachi 7 contain a buried coarse grain with a felsic composition (Cluster 2). Almost all felsic fines observed in Fig. 9 are found at the edge of these coarse grains. Some local fine-grained contamination is likely, due to erosion of coarse grains or due to laser beam edge effects, even after removing the 2 shots closest to the grain. Kenyon 10 does not contain any buried coarse grain, but is close to Kenyon 8, so the felsic fines in Kenyon 10 could be interpreted as a local contamination several millimeters away from the felsic coarse grain found in Kenyon 8. In this case the contamination could be due to the erosion of the coarse grain, "polluting" the fine-grained soil around. The same observation is made for Kanyuak 1. These observations tend to show that the LIBS transition between fine and coarse grains could occur over as many as 6 shots, or more likely that the buried felsic coarse grains in some cases contaminate the fines around them when they are eroded.

The presence of an amorphous component in the fine-grained soils (<150 μm) of the Rocknest aeolian bedform has been detected using the CheMin instrument (Bish et al., 2013) and quantified by Bish et al. (2013) and Blake et al. (2013), using data from both CheMin and APXS. They have revealed that this amorphous component represents between 27 and 45 wt% of these fines. Blake et al. (2013) have shown, by subtracting the compositions predicted from the minerals identified by CheMin from the bulk Rocknest soil observed by APXS, that this amorphous component is Si-poor (SiO_2: 37.2%), but also poor in Mg, Al and Ca content with a high Fe, Ti, Na and K content. Fine-grained soils (<150 μm) from Rock-

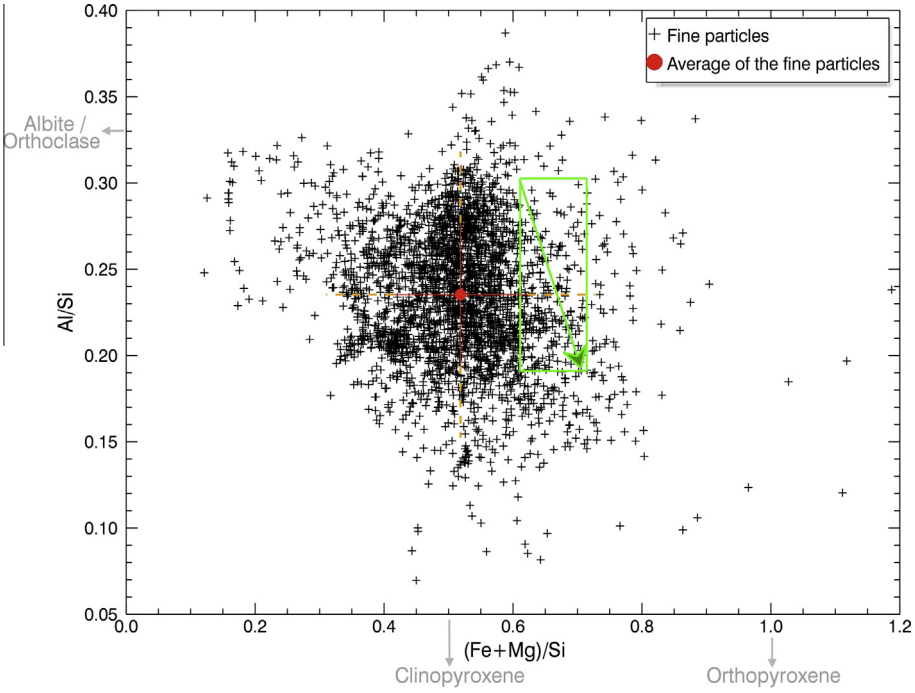

Fig. 9. Al/Si versus (Fe + Mg)/Si diagram of all the fines (molar ratios). The average and standard deviation (2σ) of all fine-grained particles spectra are shown in red/orange. Precision is comprised between this standard deviation (upper limit) and the standard deviation of the Shergottite calibration target (Fig. 8) (lower limit). The green rectangle corresponds to the range of compositions that can be obtained for a mixture in varying proportions of the crystalline and amorphous phases characterized by a combined CheMin–APXS analysis (Blake et al., 2013). The upper left (lower right) corner corresponds to a proportion of 0% (100%) of the amorphous phase. ChemCam data mimic this pattern, suggesting that ChemCam is probing varying proportions of the amorphous phase, although a systematic shift with APXS predictions is observed. (For interpretation of the references to colour in this figure legend, the reader is referred to the web version of this article.)

nest have also been analyzed by the SAM instrument, which can analyze organics and gases from the atmosphere and from solid samples. Results obtained from this analysis have shown that H_2O is bound with the amorphous component, and that the D/H ratio of these fine particles is similar to the current atmospheric value (Leshin et al., 2013). This argues against the presence in the soil of a component that would result from the alteration of rocks under hydrous conditions very different from those existing today.

This amorphous component is not directly distinguishable with ChemCam for now (probably due to its intimate mixture with crystallized fine particles). Nevertheless, fines observed by ChemCam have a low SiO_2 content in average (39.2%), and an average sum of predicted oxides of 72.8%. This suggests that they could contain some elements (H, C, S, Cl, F, P) which are not quantified yet by ChemCam, or difficult to detect by the LIBS technique. Results from CheMin, APXS and SAM instruments have shown that the total bulk contribution of SO_3, Cl, P_2O_5, Cr_2O_5, MnO, CO_2 and H_2O in the fine particles can be up to 10.8% (SO_3: 5.5 wt%, Cl: 0.6 wt%, P_2O_5: 0.9 wt%, Cr_2O_5: 0.5 wt%, MnO: 0.4 wt%, CO_2: 0.9 wt%, and H_2O: 2 wt% – Blake et al., 2013; Leshin et al., 2013), these elements being enriched in the amorphous component. If we add these contributions to the average total obtained by ChemCam, we obtain a total of predicted oxides of 83.6% (±10 wt% RMS accuracy for the major element total). The remaining missing oxides could result from the fact that the surface of the grains probed by ChemCam (only a few ng are vaporized to form the plasma) is actually enriched in S, Cl, P and H compared to their bulk values. This would be indicative of the presence of a surface coating or alteration rind enriched in these elements on the surface of the fine-grained particles. In any case, the low total and SiO_2 contents are evidence for the presence of a volatile-rich component, most likely corresponding to the amorphous phase identified by CheMin (Bish et al., 2013). Moreover, the variability in chemical compositions shown in Fig. 9 mimics the trend that could be observed for a mixture in different proportions (0–100%) of the crystalline and amorphous phases characterized by CheMin and APXS (Blake et al., 2013) (green box in Fig. 9). This further suggests that ChemCam is indeed probing different proportions of this amorphous phase. The offset between the ChemCam cluster and the green box likely reflects a systematic offset between the two techniques (ChemCam and APXS).

Hydrogen may play a role in the observed chemistry of the fines. Fig. 10 corresponds to a density diagram, representing the ratio of the H signal over the background (B, defined as the offset between the spectrum and the continuum radiation – Schroeder et al., submitted for publication), versus the SiO_2 content. Some dispersion is visible but nevertheless a trend is observed: as the SiO_2 content decreases, the H/B ratio increases. This trend means that the fines having the lowest silica values have the highest H signal, and could therefore be associated with the Si-poor amorphous phase. Points having the highest H/B values correspond to those having the lowest total oxide (<65%). This trend is also observed at the scale of the planet by the Odyssey gamma-ray spectrometer and was interpreted as the dilution, in the large field of view of that instrument, of silicate rocks by volatile-rich soils (see Fig. 19 in Gasnault et al., 2010). Investigation of some trace elements such as Cl, P and S could help to better characterize this phase. For now Cl is potentially detected in only one soil point (Kanyuak 9). S and P are still under investigation.

All these observations suggest that fine particles analyzed by ChemCam contain a portion of a Si-poor, H- and volatile-rich amorphous component. But this low total of predicted oxides, low Si content and high H signal could also be related to hydrous material (such as smectites, or hydroxides). Nevertheless, such alteration phases have not been detected in fine particles by the measurements performed at Rocknest by CheMin (Blake et al., 2013). These measurements on fine particles have been performed only at the

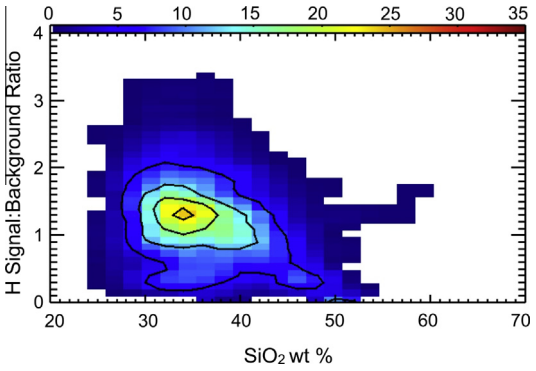

Fig. 10. Density diagram of the H signal to background ratio versus SiO_2 (wt%), for all the shots on fine particles (smaller than medium sand particles, inclusive).

Rocknest area, whereas ChemCam analyzed fine particles all along the traverse. The homogeneity in the chemistry of the fines seen by ChemCam suggests that CheMin results can be extrapolated to a broader scale and that all fines contain some fraction of amorphous phase.

4.2.2. Composition of the fines in different regions

Fig. 11 consists of seven panels for each of the most discriminative components from the ICA model. This allows comparison of each region visited by Curiosity, depending on their covariance for each of these ICA components. Each of the three regions overlaps in composition with the others, meaning that they are very similar. Moreover, their medians are very comparable. This means that the fines are very similar in all regions, consistent with Fig. 9. Nevertheless, the distributions slightly differ depending on the region and the elemental component. Rocknest and Yellowknife Bay have more variability for Si, Mg and Fe, both for the high and the low values. The distributions are sometimes asymmetric, for example at Bradbury for the Fe component, with a median very close to the lower quartile, which may indicate a small contribution by a Fe-rich component.

Some outliers are observed. High-side outliers are observed for all the components, whereas low-side outliers are observed only for the Mg component. The outliers and variability with high values for the components Si, Na, Al and K are related to the felsic fines observed in Fig. 9: Kenyon points 8 and 10, Kanyuak 1 and Pachi 7 are usually outliers in the high values for Al, Si, and also Na and K components. Two outliers for the Fe component at the Bradbury site are observed, and they correspond to the fines encountered at Murky 3 and Kam 4. These locations also revealed the presence of a buried coarse grain, having a Cluster 3 composition, enriched in Fe. So this enrichment in Fe in these fine particles could be due to a contamination from these buried grains encountered deeper at both locations (due to coarse-grain erosion or to laser beam edge effects).

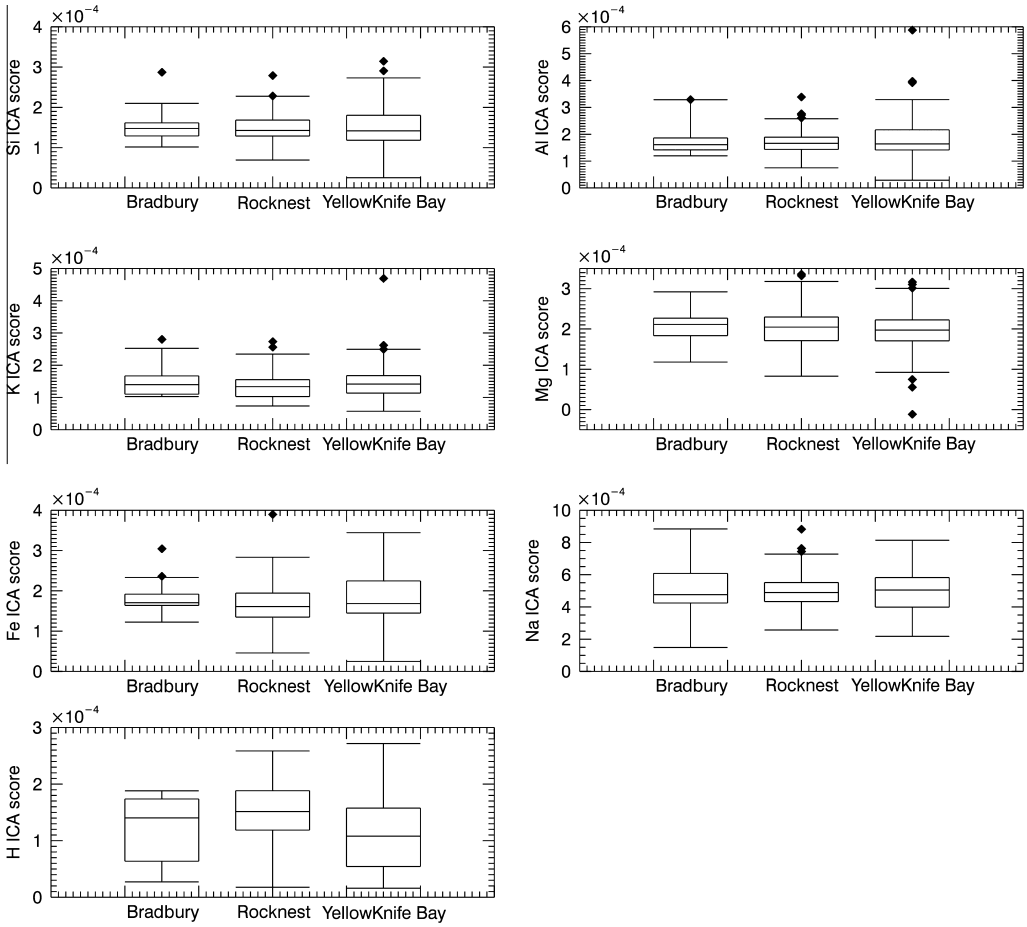

Fig. 11. Boxplot representation for each principal ICA score, obtained on the average of the fines acquired on each point location. Results are presented for each region (Bradbury, $n = 12$; Rocknest, $n = 66$; Yellowknife Bay, $n = 57$). The line inside the box represents the median value of the dataset. Upper and lower lines of the box represent the higher and lower quartile, respectively. Whiskers represent the maximum and minimum value, still within 1.5 times the interquartile range of the higher and lower quartile, respectively. Black points are outliers; they are defined as: top outliers have a value higher than the interquartile range of the higher quartile (> higher quartile + 1.5 × [higher − lower quartiles]), whereas low outliers are lower than the interquartile range of the lower quartile (< lower quartile − 1.5 × [higher − lower quartiles]).

Regarding the H component, medians are relatively similar but with some differences: the median at Rocknest is slightly higher (best correlation with H component) with the smallest variability, whereas Yellowknife Bay fines have the lowest median. Fines from Yellowknife Bay and Bradbury have a relatively similar distribution. No outliers are observed for the H component in each area. One hypothesis to interpret the higher correlation with H at Rocknest area could be that the fines analyzed at the Rocknest aeolian ripple have a smaller size than the other fines encountered at other locations, and thus a larger (hydrated) surface/volume ratio. Laboratory measurements could be very useful to test this hypothesis.

Overall, although some chemical variability is observed, the fine particles analyzed by ChemCam over 2660 shots appear quite homogeneous, which is consistent with the idea that this material is regionally to globally distributed by aeolian processes, and is thus homogenized, or that their source materials are widespread and typical of the surface of Mars, and possibly more sensitive to weathering. In some cases there is evidence for some local contamination from coarse grains. However, the small overall chemical heterogeneity observed for the fine particles, known to vary in color, size and shape (Goetz et al., 2010), and their basaltic composition, suggests limited chemical, or isochemical alteration of the fine soil constituents and limited interaction with liquid water, in agreement with previous investigations (Goetz et al., 2005; Yen et al., 2005; Pike et al., 2011; McGlynn et al., 2012).

5. Discussion

5.1. Compositional difference between fine and coarse grains

Fig. 12 shows a histogram of individual spectra of coarse grains and fine particles, representing the frequency versus the score of principal ICA components corresponding to the element of interest. As discussed earlier, hydrogen is a strong distinguisher of fines. The fines (dashed lines) show more spectra with a higher covariance for the H component than coarse grains (score is 1.3×10^{-4} for 2735 fines spectra, compared to a mean of 0.54×10^{-4} for 77 coarse-grain spectra). The H peak in the LIBS spectra has not yet been quantified, except at Rocknest by comparison to SAM Evolved Gas Analysis (Leshin et al., 2013; Meslin et al., 2013). Even if the H line is subject to matrix effects (Schroeder et al., submitted for publication), Fig. 12 confirms that the fines have a higher H signal than the coarse grains. Moreover, this is consistent with the fact that the felsic coarse grains (Cluster 2) show the lowest H signal, which is consistent with these being feldspars, which are anhydrous minerals.

Cluster 2 of coarse grains shows a higher score with the Al, Si, Na, and K components than other coarse grains and than the fines. It also has a lower score for the Fe and Mg components. These trends are consistent with a felsic composition. Cluster 3 always shows a higher score with these components than the fines and Cluster 1, even if it has a lower score than Cluster 2. Cluster 3 also shows a higher covariance to the Fe and Ti components than other coarse grains and than the fines, which supports the fact that this group is not a mixture of the two other clusters. Nevertheless the highest correlation with Ti is observed for a coarse grain from cluster 1, corresponding to Shezal point 4, and this is consistent with the PLS1 quantitative results.

Another observation can be made from Fig. 12: coarse grain Cluster 1 is similar to the fines for all the elements presented here. Some of these Cluster 1 coarse grains also have a relatively strong H component, comparable to that of the fines. Moreover, the average major element total for Cluster 1 is very low, as also found for the fine particles (~73% for Cluster 1, ~76% for fines in average). Several hypotheses can be proposed:

(i) Coarse grains from Cluster 1 may not be truly individual coarse grains. They could represent aggregates of fine particles. In this case, Cluster 1 would correspond directly to indurated fines. These fines can be agglomerated in several ways: they can be cemented or this agglomeration can result from a recrystallization of the fines. In any case the material that binds the fine particles together has the same chemistry as the fines or is a minor constituent. One issue with this hypothesis is that one should explain why this cementing process has affected only a very small fraction of the fines, and is not more frequently found.

(ii) Coarse grains in Cluster 1 could be precursor materials to the fines. Fines and coarse grains in Cluster 1 share a similar composition and a very low major element total. This low total for coarse grains from Cluster 1 suggests that they have undergone some alteration and could contain some volatile-rich amorphous phase as well. This hypothesis implies that these coarse grains from Cluster 1 are mechanically weathered during their transport, "loosing" part of their mass, which, by mass balance, must create the fine particles in much greater number. Isochemical weathering can also contribute to the formation of fine particles. The similar composition between fines and coarse grains in Cluster 1 could therefore also result from isochemical alteration of similar mineral phases. Consequently, the amorphous phase observed in the fines by CheMin (Bish et al., 2013) could have different origins: it could have formed as part of these coarse grains and transferred to finer separates by physical weathering, or it could have formed directly by isochemical alteration of the fines.

Detection of coarse grains in the soil is important to better constrain the soil production/origin on Mars, as it was shown here that most of the coarse grains have compositions that differ from the composition of the fines. To investigate this aspect further, the ratio between the fines and all soil observations made by ChemCam is shown in Fig. 13. Here the average soil composition was calculated from all the soils analyzed by ChemCam up to Yellowknife Bay, with no distinction between fines and grains. Pebbles, coarse grains and fine particles are mixed together. This comparison shows that this average is enriched mostly in silica, aluminum, calcium and alkali compared to the fines, whereas the latter are mostly enriched in titanium, iron and magnesium compared to the soils in general. Similarly, Table 3 shows the compositions of Portage, an APXS soil standard measured in a wheel track of the Rocknest area, along with soils observed by ChemCam, where the contributions of coarse grains and fines were separated. Comparison between APXS soil composition and ChemCam fine particle composition shows that ChemCam major element estimations are always lower than those of APXS. Nevertheless, taking into account the uncertainties and the differences in normalization (APXS values are hydrogen and carbon-free compositions), compositions from both techniques overlap in most cases. Disparities are still observed for Fe, Mg and to a lesser extent, Na. This is also apparent in the lower sum of oxides. This could be mostly explained by intrinsic differences between the two techniques, or this could also partly result from the fact that ChemCam is seeing larger proportions of volatiles elements (S, Cl, H), which would lower the proportions of other elements. It is also noteworthy that the APXS value for FeO at Portage is high compared to MER soils (around 19% compared to 17% for the MER values (Taylor and McLennan, 2009)), and that Rocknest coarse grains are found to be mostly from Cluster 3 and therefore are enriched in Fe compared to the fines.

A portion of the scooped and sieved material used for the CheMin and SAM analyses was deposited on the titanium science observation tray (Otray) in order to measure the <150 μm-size

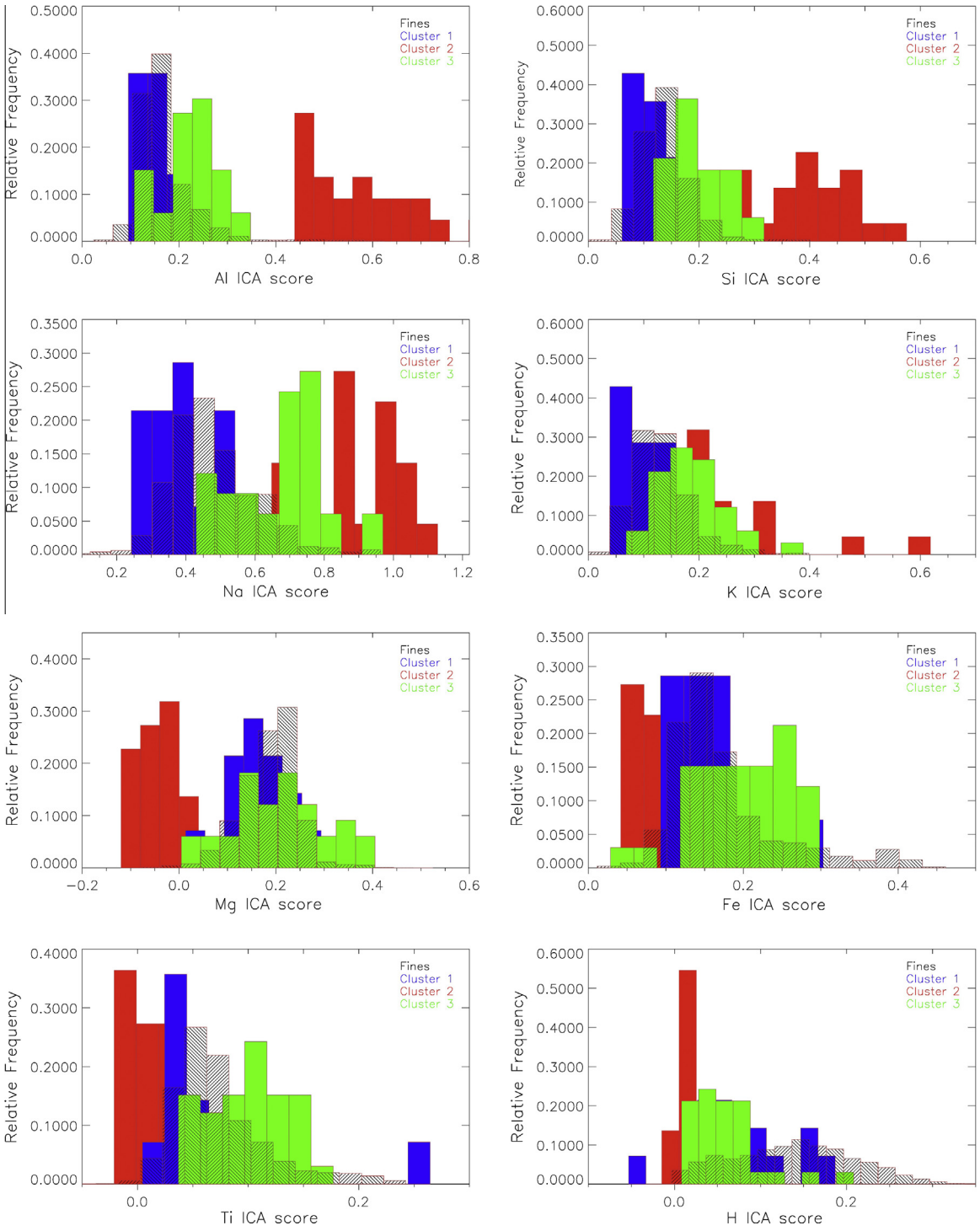

Fig. 12. Histogram of the distribution of the spectra for several ICA components, for the fines and each cluster of coarse grains. ICA scores are multiplied by 10^{-3} for clarity.

particles with APXS (Berger et al., 2013). APXS results indicate that the particulate on the Otray had a similar composition to the soil *in situ*, except for enrichment in S. The Otray sample was thin with respect to the APXS information depth for Mn and Fe (Campbell et al., 2009), and oxide concentrations could not be calculated using the standard APXS calibration method. Therefore, quantifying a difference in composition between the finer sieved material on the Otray and the coarser *in situ* grains in the APXS field of view (Fig. 14) was not possible with the two APXS measurements.

The average martian soil composition (Taylor and McLennan, 2009) is also reported in Table 3, together with the average composition of each group of coarse grains. For most major elements, this martian soil composition falls between Clusters 1 and 2 compositions. This suggests that the bulk chemical analyses of martian soils could be influenced by the presence of coarse grains. To summarize, the similarity in composition of soils at Rocknest compared to other soils analyzed on Mars conceals a diversity in grain composition that ChemCam is able to analyze.

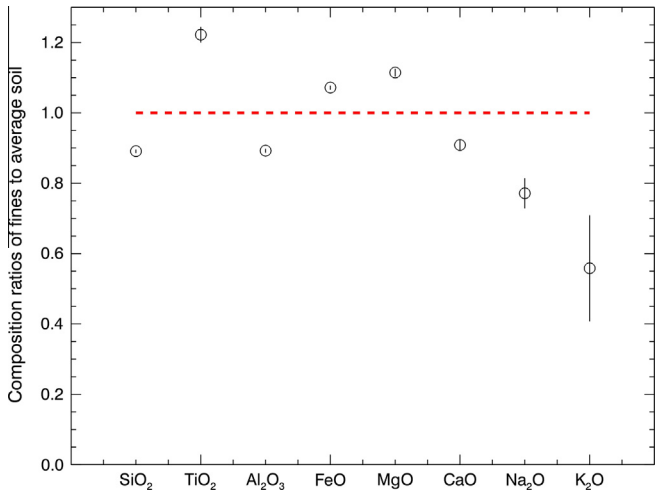

Fig. 13. Ratio between the fines and the average soil composition from the ChemCam analyses. Error bars represent the precision for each element, using all the data obtained on the Shergottite calibration target onboard Curiosity, at 40 Amps.

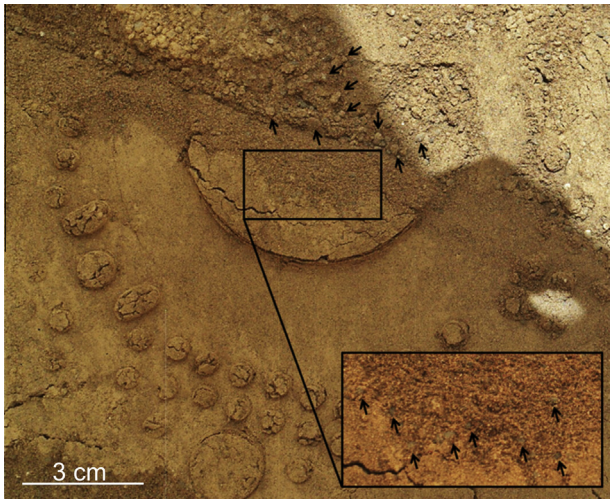

Fig. 14. The soil Portage as imaged by MAHLI and investigated by APXS (both on sol 89). Note the high-fidelity casting of the APXS contact plate (including the larger screw hole on the very bottom). Arrows mark some of the coarse grains within the field of view of the APXS, which was about 3.1 cm in diameter at a standoff distance of 2 cm. Image ID: Background image: Detail of 0089MH0120001001E1. Top insets: 0089MR0628000000E1 and 0089MR0629000000E1. Bottom inset: Detail of 0089MH0122001001E1.

5.2. Coarse grains origin

Three kinds of coarse grains have been distinguished by their chemistry. Coarse grains in Cluster 2 are mainly observed at the Bradbury rise whereas Clusters 1 and 3 are observed all along the traverse. The objective of this section is to investigate the relationship between coarse grains and the rocks encountered at Gale.

Coarse grain Cluster 2 has been observed mostly at the Bradbury site. A Sammon's map representation including all the coarse grains of Cluster 2, and all the rocks (each single location, mainly on float rocks at Bradbury and mainly bedrock at Yellowknife Bay) for each unit analyzed by ChemCam, shows that overall coarse grains in Cluster 2 (red diamonds) are close to the Bradbury rocks (orange[1] circles) (Fig. 15). In greater detail, the closest rocks are Link (points 1, 2, 3 and 4), Mara 1st point and point 4, Preble points 1 and 2, Thor Lake 1, 2 and 3, Goulburn 4 (Sautter et al., 2013) and Jake_M (points 3, 10). Link is a conglomerate with a clear felsic composition, which could suggest that some of the coarse grains observed are from pebbles contained in this conglomerate (Sautter et al., 2013). This is the case for Beechey 2 and 5, Kam 6 and even McTavish 2, which was observed in the quite distant Yellowknife Bay unit. Concerning other pebbles/coarse grains observed at Yellowknife Bay, Kanyuak 5 is close to Thor Lake 2 and Stark, which are alkali-rich rocks (Sautter et al., 2013); Kanyuak 1 is close to other grains (Pachi 7 and 9), and the closest rock is Link3 and Preble 1, also with a felsic composition (Sautter et al., 2013). However, Kanyuak 3 is not so close to any rocks and the closest coarse grains are Kanyuak 1 and Pachi 7. The closest rock is Goulburn 7, which was also enriched in felsic components.

Moreover, looking at the distribution of the Cluster 2 coarse grains along the traverse, most of them are visible at the surface (59%). At the Bradbury site, 83% of the coarse grains observed in Cluster 2 are exposed at the surface, and this proportion decreased as the rover approached the Yellowknife Bay unit, a greater proportion of coarse grains being buried there. Observation of coarse grains in Cluster 2 at the surface of the Bradbury rise tends to show that these coarse grains are similar to the Bradbury rocks. This suggests that those pebbles and coarse grains could result from local alteration at Bradbury rise, and/or could originate from the same source as the float rocks encountered at Bradbury. The Bradbury site is located at a distal portion of Peace Vallis alluvial fan, which transported material from the northern crater rim toward the landing site area (Palucis et al., submitted for publication).

The origin of coarse grains Clusters 1 and 3 is more difficult to decipher. The Sammon's representation that includes these coarse grains as well as all the rocks analyzed by ChemCam (Fig. 16) shows that coarse grains in Cluster 1 (red diamonds) are relatively close to the rocks analyzed at Point Lake (mainly bedrock), which is an outcrop observed in the Glenelg member of Yellowknife Bay (dark green rocks; Anderson et al., submitted for publication), and coarse grains in Cluster 3 are mostly close to the Sheepbed rocks in Yellowknife Bay (which correspond to bedrock), even if they show much more variability. An ICA-based clustering tool applied to ChemCam LIBS observations (Gasnault et al., 2013) is consistent with the Sammon's map observations: Cluster 1 groups together with mainly rocks observed in Point Lake outcrop (but also some Sheepbed and Gillespie rocks), whereas coarse grains in Cluster 3 are in the same group (Sheepbed rocks) but with much more sub-groups, because of their variability. The Sheepbed member is the lowest stratigraphic member of Yellowknife Bay (Grotzinger et al., submitted for publication). It corresponds to fine-grained sediments with some sulfate-bearing fracture filling (Nachon et al., submitted for publication) and also diagenetic features such as nodules or raised-ridged (Léveillé et al., submitted for publication). A shallow lacustrine environment is proposed as the formation setting for this unit (Grotzinger et al., submitted for publication). Point Lake outcrop is part of the Glenelg member. Rocks observed in this area are mostly dark with several kinds of rough textures. One hypothesis concerning the formation of this outcrop refers to a volcanic flow, even if this hypothesis does not seem consistent will all the observations (Mangold et al., submitted for publication).

The fact that coarse grains in Clusters 3 and 1 are similar in composition to Point Lake outcrop and Sheepbed bedrocks does not necessarily mean that they originate from these rocks, because they are both close to the martian crust average. Moreover, all the coarse grains in Cluster 1 and 64% of the coarse grains in Cluster 3 are buried. This is in favor of the hypothesis that they have been transported and then buried by aeolian processes (if they are local

[1] For interpretation of color in Figs. 15 and 16, the reader is referred to the web version of this article.

Table 3
Comparison of ChemCam results (PLS1) and APXS results at the Rocknest sand shadow. (*) From Blake et al. (2013), (**) from Taylor and McLennan (2009), (***) Difference (Reference Total) – (Sum of oxides not quantified by PLS1) – (Sum of oxides from PLS1); for the Rocknest analyses performed by ChemCam, the reference total refers to the Portage total of oxides performed by APXS; for the three groups distinguished by ChemCam analyses, the reference total corresponds to the Average martian Soils. This residual is partly due to the difference in normalization between the two techniques (APXS values are normalized to 100 wt% on a water- and carbon-free basis, whereas PLS1 values are not normalized to 100 wt% in order to be able to predict unknown component (like minor and traces elements). Standard deviations are given in parentheses for the PLS1 results, for each group/category observed by ChemCam.

	Portage APXS*	Mean coarse grains CCAM Rocknest	Average fines CCAM	Average martian soil**	Felsic group	Intermediate group	Mafic group	RMSEP (PLS)
SiO_2	42.88 ± 0.47	44.9 (7.77)	37.1 (5.94)	45.41	67.1 (9.01)	45.9 (5.31)	35.3 (3.84)	7.1
TiO_2	1.19 ± 0.03	1.4 (0.34)	1.3 (0.18)	0.9	0.8 (0.28)	1.2 (0.34)	1.5 (0.45)	0.55
Al_2O_3	9.43 ± 0.14	8.9 (2.39)	7.4 (1.67)	9.71	15.7 (2.78)	8.6 (1.76)	6.1 (1.37)	3.7
FeOT	19.19 ± 0.12	14.2 (3.98)	12.9 (2.7)	16.73	9.6 (3.23)	15.3 (3.17)	11.7 (2.13)	4
MgO	8.69 ± 0.14	4.6 (2.90)	5.4 (2.1)	8.35	3.5 (3.45)	4.7 (2.84)	7.6 (1.76)	3
CaO	7.28 ± 0.007	7 (6.54)	6.8 (2.04)	6.37	4.4 (3.09)	7.1 (3.20)	8.6 (2.47)	3
Na_2O	2.72 ± 0.1	1.9 (0.79)	1.6 (0.62)	2.73	4.4 (0.82)	2.2 (0.57)	1.3 (0.41)	0.7
K_2O	0.49 ± 0.01	0.7 (0.49)	0.3 (0.27)	0.44	1.8 (0.79)	0.7 (0.59)	0.4 (0.34)	0.9
Cr_2O_3	0.49 ± 0.02			0.36				
MnO	0.41 ± 0.01			0.33				
P_2O_5	0.94 ± 0.03			0.83				
SO_3	5.45 ± 0.1			6.16				
Cl	0.69 ± 0.02			0.68				
Sum of oxides not quantified by PLS1	7.98			8.36				
Residuals***		8.37	19.07		−16.7	4.9	18.1	
Total	99.85	83.5	72.8	99	107.3	85.7	72.5	

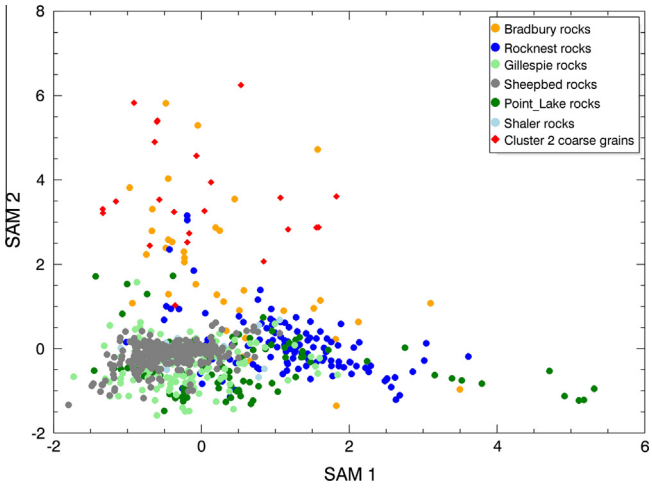

Fig. 15. Sammon's map with all the rocks observed in each unit and the Cluster 2 coarse grains observed. Pebbles are in diamond whereas the rocks are represented by circles. Shaler and Point Lake are outcrops from the Glenelg member at Yellowknife Bay. No distinction is done between floats and bedrocks here.

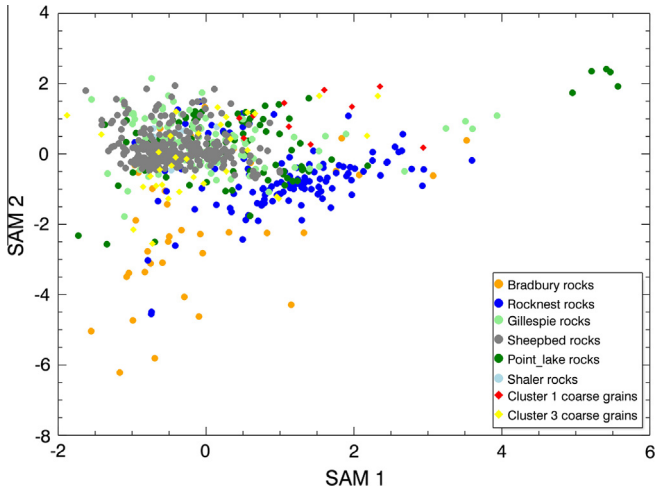

Fig. 16. Sammon's map with all the rocks observed in each unit and coarse grains from Cluster 1 and Cluster 3. Pebbles are represented by diamonds whereas the rocks are represented by circles. Shaler and Point Lake are outcrops from the Glenelg member at Yellowknife Bay. No distinction is done between float rocks and bedrock here.

but buried, this would mean that there is no mechanical weathering anymore of their source rocks, contrary to BradBury Rocks). Furthermore, if the coarse grains in Cluster 1 are associated with the fines, their origin is therefore more difficult to understand, as with the global martian soils.

Some examples are presented to illustrate the relationship between coarse grains in Clusters 1 and 3 and the local rocks: in the Rocknest area, coarse grains and pebbles are clearly different from the rocks encountered in this area. The coarse grains in this area are mostly part of Cluster 3 (others are part of Cluster 1). Rocknest rocks contain more Fe and less Mg than the coarse grains of this region. Those coarse grains also contain more Si and Na compared to the rocks. From these observations, we can conclude that the coarse grains forming the Rocknest bedform armor are different from the rocks analyzed in this area. This is consistent with the hypothesis that the bedform armor coarse grains are not from mechanical alteration of the local rocks from this area, but have been transported from another region (Meslin et al., 2013). It is also consistent with the results from the Sammon's map and from the clustering analysis (discussed above).

In the Yellowknife Bay area, ChemCam analyzed a rock called Nanok twice, on sols 176 and 184. This rock was particularly interesting, as it corresponds to a bedrock broken by the rover wheels, thereby exposing a fresh surface (Fig. 17). Nanok presents some interesting features: patches of light-toned material (likely residual sulfate vein material) inside a relatively dark-toned sandstone, and a passive spectral signature consistent with a deficiency of crystalline ferric oxides (Johnson et al., 2015). Nevertheless the composition of the freshly exposed part (data from sol 184 only) is homogeneous, with an overall basaltic composition. The light-toned material was not sampled. Very close to this rock (at ~12 cm), ChemCam analyzed a soil called "Sutton Inlier", which was disturbed by the rover wheel. These analyses were aimed at investigating the presence of coarse grains mixed within it (which was suspected by the unusual shape of the laser pits in that soil),

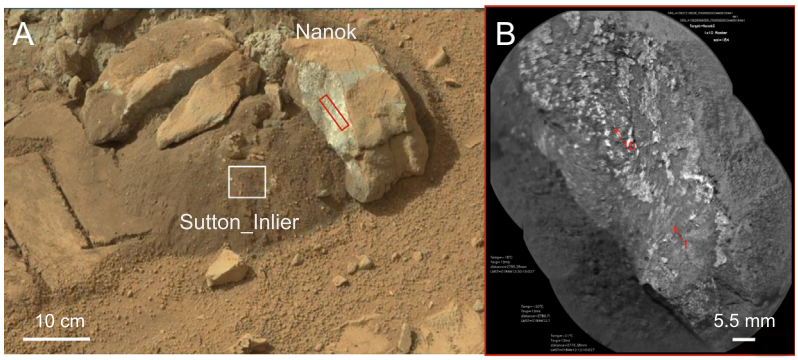

Fig. 17. (A) MastCam Left image ("0192ML1019024000E1_DXXX") taken during sol 192, showing the Nanok float rock (observed at Yellowknife Bay area) with a fresh broken surface and the Sutton Inlier disturbed soil. The passage of the rover wheel over the rocks pushed up the disturbed soil, created the exposed rock face on Nanok and resulted in rover tracks that are visible on the left. (B) RMI Mosaic (Le Mouélic et al., 2015) of the fresh surface of the Nanok rock, where ChemCam analyses were performed. Points 1 and 10 represent the first and last ChemCam point analysis, respectively. Credit: NASA/JPL-Caltech/MSSS.

and if the coarse grains could originate from the Nanok rock. This soil was a very fine-grained soil and therefore only two buried coarse grains were detected over eight analyzed locations in total (one coarse grain on the first location and a second one on the fourth location). Both coarse grains are part of Cluster 3. Their composition is different from Nanok, mostly because they are richer in Si, Na and Al, and have overall less Fe. This observation is another example illustrating the fact that coarse grains at Yellowknife Bay do not seem to derive from local rocks.

To assess the origin of the coarse grains, trends in minor and trace elements can also be investigated. Fig. 18 shows the estimates for some trace elements (Sr, Ba and Rb; Ollila et al., 2013), peak areas for Cr and Mn (not yet calibrated for abundances) and estimates (from PLS1 technique) of K and Ca contents. This figure presents the results obtained for several categories of targets: the three groups of coarse grains and a selection of rocks which are close to each group in the Sammon's map representations (Figs. 15 and 16), namely the Bradbury rocks, some of the Sheepbed rocks (Ca sulfates are removed) and some of the Point Lake outcrop.

Ba and Rb are elements that can substitute for K, as they are associated with alkali feldspars, and Sr can substitute for K and Ca as it is associated with alkali feldspars and plagioclase. In

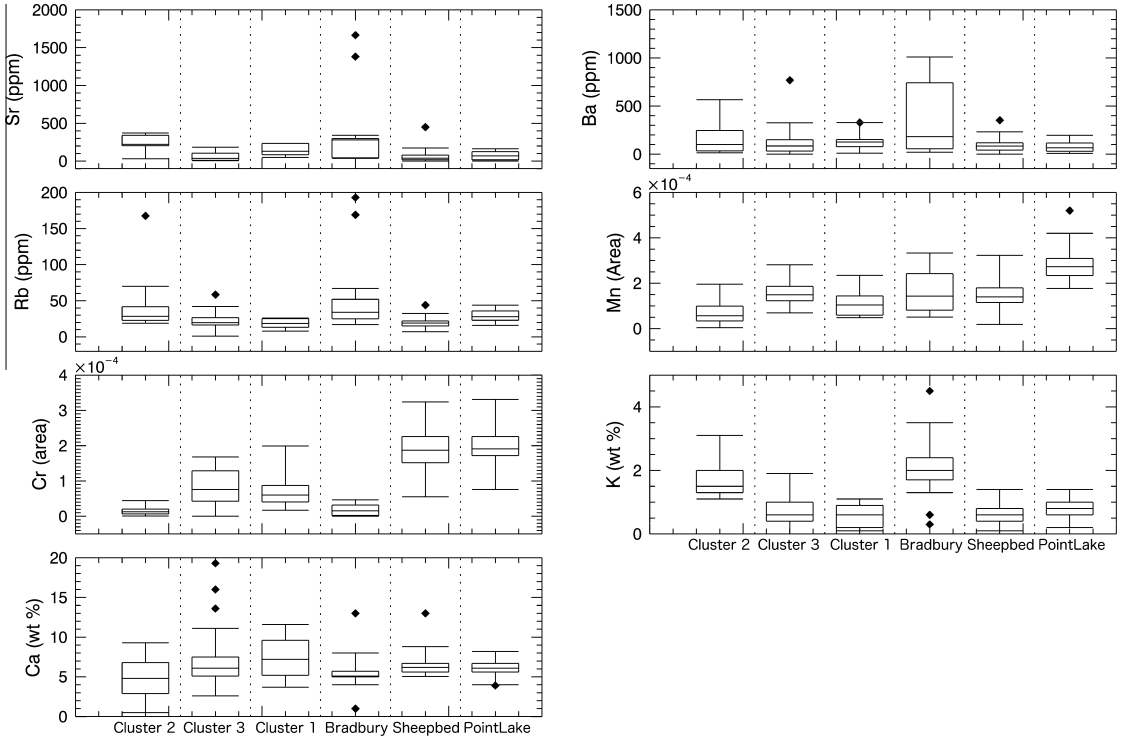

Fig. 18. Boxplot representing the distribution of some trace elements (Sr, Rb, Ba) in ppm, Cr and Mn (peak areas; not yet calibrated for abundance) and distribution of K and Ca in wt%, for each cluster of coarse grains (Cluster 1, $n = 15$; Cluster 2, $n = 22$; Cluster 3, $n = 40$) and each associated rocks susceptible to be their source of origin (Bradbury, $n = 9$, Sheepbed, $n = 323$, Point Lake, $n = 15$). Sheepbed and Glenelg (which encompasses the Point Lake outcrop) are two members of Yellowknife Bay (Grotzinger et al., submitted for publication). The derived values for these trace elements can be negative, within the RMSEP: 160 ppm for Sr, 624 ppm for Ba, 44 ppm for Li, and 33 ppm for Rb (Ollila et al., 2013). The line inside the box represents the median value of the dataset. Upper and lower lines of the box represent the higher and lower quartile, respectively. Whiskers represent the maximum and minimum value, still within 1.5 times the interquartile range of the higher and lower quartile, respectively. Black points are outliers; they are defined as: top outliers have a value higher than the interquartile range of the higher quartile (> higher quartile + 1.5 × [higher − lower quartiles]), whereas low outliers are lower than the interquartile range of the lower quartile (< lower quartile − 1.5 × [higher − lower quartiles]).

Fig. 18, Sr, Rb and Ba in the Bradbury rocks and Cluster 2 have the highest median and even show some high outliers. This cluster is different from all the other clusters of coarse grains. Moreover, the Bradbury rocks have the highest median for Ba, with a large distribution toward high values. The median of the felsic coarse grains is not as high, but this category also has a wide distribution in high Ba content. Cluster 2 and Bradbury rocks also show the highest median for K_2O, which is consistent with the observations for Sr, Ba and Rb. Nevertheless, Cluster 2 and Bradbury rocks do not show the highest median for Ca, which is not consistent with the Sr observations. This implies that the Sr detected in Cluster 2 coarse grains and in Bradbury rocks is mainly associated with alkali feldspars and not Ca-rich plagioclase. Concerning these alkali feldspar-associated elements (Rb, Ba, Sr, K), Clusters 1 and 3 show a lower median than Cluster 2, and also show a narrower distribution. They also present relatively similar contents compared to Sheepbed and Point Lake rocks (respectively). This can be explained by the fact that these trace elements are observed mainly in feldspars, which are not observed in those coarse grains and in the rocks encountered at Sheepbed and Point Lake. Therefore the origin of Cluster 1 and Cluster 3 coarse grains cannot be assessed with certainty from this analysis.

Regarding Cr, coarse grain Cluster 2 and Bradbury rocks show the lowest peak areas compared to other coarse grains and other rock units, as with Mn but to a lower extent. This is consistent with the results obtained from other minor and trace elements, since Cr and Mn are mainly present in minerals such as pyroxenes and olivines, and not in feldspars. Coarse grains Cluster 3 is enriched in Cr and Mn compared to other coarse grains, which is consistent with the fact that these points do not represent a mixing between Clusters 1 and 2. Moreover, the Cr content in Clusters 1 and 3 is clearly lower than those observed at Yellowknife Bay (Sheepbed member and Point Lake outcrop). The same observation is made for the Mn content of Cluster 1. These differences in Cr and Mn contents are key to deducing that the Point Lake outcrop and Sheepbed rocks do not represent the parent material of Clusters 1 and 3, respectively.

To conclude on the origin of the coarse grains, we suggest that Cluster 2 has the same source as the Bradbury float rocks, whereas coarse grain Clusters 1 and 3 seem to predominantly have an origin different from all the rocks analyzed during the first 250 sols of the mission, although their share chemical similarities with some float/bedrocks.

6. Conclusion

ChemCam observed 24 soil targets and 172 LIBS points during the first 250 sols. At each of these locations the analysis was made to a depth of a few millimeters, in strong contrast to all previous observations on Mars. As the footprint is smaller than that of the APXS, we are able to distinguish pebbles and also buried coarse grains from fine particles, and thus to establish a relationship between grain size and chemical composition. This study has revealed several points, which are summarized below.

Among all the soil targets sampled, 45% of them revealed the presence of a coarse grain, 86% of which were buried. At least 3 groups of pebbles/coarse grains were distinguished. The coarse grains in Clusters 1 and 2 are quite homogeneous, whereas Cluster 3 shows more diversity.

Coarse grains in Cluster 2 were encountered mostly in the Bradbury region. These coarse grains have a felsic composition and seem to have the same source as the Bradbury float rocks and conglomerates. As these coarse grains are observed at the surface at Bradbury site, it is possible that some of these coarse grains come from local physical weathering of these rocks. In contrast, coarse grains encountered at Rocknest are different from the rocks analyzed in this region. These rocks, except the felsic ones and the fluvial conglomerates, do not seem to have contaminated the soil (either as coarse or fine particles). This could suggest that these rocks are more resistant to the type of mechanical weathering that results in small clasts or pebbles, perhaps due to the fine-grained nature of these rocks. The non-felsic coarse grains (Clusters 1 and 3) seem to have been transported to the present location at an earlier time, as they are mostly buried (except those encountered in the bedform armor of Rocknest). Coarse grains in Cluster 1 could be agglomerates of fine particles, or more probably directly involved in the process of fines formation. This could explain their similarity in composition and their larger hydrogen signal. Coarse grains from Cluster 3 seem to be mostly derived from a source with a specific composition enriched in Cr and Mn.

The observation of some contamination of the fine particles by coarse grains having a felsic composition (Cluster 2) suggests that sometimes the local material has been weathered and has produced fine particles. Fines are very homogeneous, but different in composition from the rocks encountered at Gale crater by ChemCam along the traverse. This is consistent with multiple studies from previous missions (Yen et al., 2005), showing that martian soils have a composition different from all the rocks analyzed so far. Therefore the question of their origin remains open. They may represent a mixture of different chemical components whose composition, although close to the average martian crust, does not resemble that of any specific rock types. This systematic difference probably stems from the presence of the volatile-rich amorphous phase identified by CheMin (Bish et al., 2013; Blake et al., 2013). McSween et al. (2010) suggested that such a combination could result from the physical mixing of two unrelated components of different ages and origin: one derived from relatively young olivine-rich basalts, and one derived from the alteration of ancient rocks under hydrous conditions. Those two unrelated components, however, would probably be carried by different particles (possibly with different sizes), whose relative abundance is very likely to vary from place to place. However, if the fine particles are derived from the mechanical weathering of altered coarse grains (Cluster 1), the mixture between the amorphous phase and the igneous minerals could be more intimate than in the previous scenario. To discriminate between these two scenarios, future investigations will try to decipher whether the amorphous phase is intimately mixed with the igneous minerals (i.e. at very fine scale), or whether it is carried by several types of materials that could be separated in a ChemCam analysis. However, if the low totals obtained with ChemCam on the fine-grained and on a few coarse-grained particles result from the presence of an amorphous coating enriched in S, Cl, P and H_2O, the scenario of two unrelated components would be refuted. Moreover, the D/H signature of the water released during SAM Evolved Gas Analysis (EGA) of Rocknest samples, found to be similar to the current atmospheric value (Leshin et al., 2013), seems to argue against the presence in the soil of a component that would result from the alteration of rocks under hydrous conditions very different from those existing today, in contrast to the scenario proposed by McSween et al. (2010).

ChemCam analyses of fine particles are consistent with the presence of an amorphous component mixed with these fine-grained soils, as shown by CheMin results (Bish et al., 2013). These fine particles have a low total of predicted oxides. Moreover, their H abundance seems to be controlled by the abundance of the amorphous phase, as revealed by the H versus SiO_2 anti-correlation. However, the overall chemical homogeneity of the fine particles, close to basaltic composition, and the lack of strong alteration trends in ChemCam data suggest limited or isochemical alteration and limited interaction with liquid water.

ChemCam data show that the bulk chemistry hides a strong variability in mineralogy due to a mixing between grains eroded from local rocks and grains transported by wind. Thus, soils with a composition close to the martian crust can be the result of the mixing of multiple sources and not just the result of a single source with an average martian composition.

Acknowledgments

NASA's Mars Program Office sponsored this research. The whole team acknowledges JPL for developing and leading this successful mission. The team also acknowledges CNES for its important role shared in the ChemCam operations. The data reported in this paper are archived at the Planetary Data System, accessible at http://pds-geosciences.wustl.edu/missions/msl/index.htm.

Appendix A. Supplementary material

Supplementary data associated with this article can be found, in the online version, at http://dx.doi.org/10.1016/j.icarus.2014.04.052.

References

Anderson, R.B. et al., 2013. Chemistry of the Shaler outcrop investigated by ChemCam. Icarus (submitted for publication).
Aragon, C., Aguilera, J.A., Penalba, F., 1999. Improvements in quantitative analysis of steel composition by laser-induced breakdown spectroscopy at atmospheric pressure using an infrared Nd:YAG laser. Appl. Spectrosc. 53, 1259–1267.
Baird, A.K. et al., 1977. The Viking X-ray fluorescence experiment: Sampling strategies and laboratory simulations. J. Geophys. Res. 82, 4595–4624.
Bandfield, J.L., Hamilton, V.E., Christensen, P.R., 2000. A global view of martian surface compositions from MGS-TES. Science 287, 1626–1630.
Bell, J.F. et al., 2000. Mineralogic and compositional properties of martian soil and dust: Results from Mars Pathfinder. J. Geophys. Res. 105, 1721–1756.
Berger J.A. et al., 2013. MSL titanium observation tray measurements with APXS. Lunar Planet. Sci. 44. Abstract #1321.
Bish, D. et al., 2013. X-ray diffraction results from Mars science laboratory: Mineralogy of Rocknest at Gale crater. Science 341. http://dx.doi.org/10.1126/science.1238932.
Blake, D.F. et al., 2013. Curiosity at Gale crater Mars: Characterization and analysis of the Rocknest sand shadow. Science 341. http://dx.doi.org/10.1126/science.1239505.
Blaney et al., 2013. Chemical and textural variability among rocks observed at Rocknest, Gale crater. J. Geophys. Res. (submitted for publication).
Brückner, J., Dreibus, G., Rieder, R., Wänke, H., 2001. Revised data of the Mars pathfinder alpha proton X-ray spectrometer: Geochemical behavior of major and minor elements. Lunar Planet. Sci. 32. Abstract #1923.
Campbell, J.L. et al., 2009. A fundamental parameters approach to calibration of the Mars Exploration Rover alpha particle X-ray spectrometer. J. Geophys. Res. 114. http://dx.doi.org/10.1029/2008JE003272.
Chaléard, C., Mauchien, P., André, N., Uebbing, J., Lacour, J.L., Geertsen, C., 1997. Correction of matrix effects in quantitative elemental analysis with laser ablation optical emission spectrometry. J. Anal. At. Spectrom. 12, 183–188.
Clark, B.C., Baird, A.K., Weldon, R.J., Tsusaki, D.M., Schnabel, L., Candelaria, M.P., 1982. Chemical composition of martian fines. J. Geophys. Res. 87, 2156–2202.
Clegg, S., Sklute, E., Dyar, M.D., Barefield, J.E., Wiens, R.C., 2009. Multivariate analysis of remote laser-induced breakdown spectroscopy spectra using partial least squares, principal component analysis, and related techniques. Spectrochim. Acta Part B 64, 79–88.
Cousin, A. et al., 2011. Laser-Induced Breakdown Spectroscopy (LIBS) library under martian environment. Spectrochim. Acta Part B 66, 805–814.
Cremers, D.A., Radziemski, L.J., 2006. Handbook of Laser-Induced Breakdown Spectroscopy, first ed. Wiley, England.
Duda, R.O., Hart, P.E., 1973. Pattern Classification and Scene Analysis, first ed. Wiley, New York.
Fabre, C. et al., 2011. Onboard calibration igneous targets for the Mars science laboratory Curiosity rover and the chemistry camera laser induced breakdown spectroscopy instrument. Spectrochim. Acta Part B 66, 280–289. http://dx.doi.org/10.1016/j.sab.2011.03.012.
Fabre, C. et al., 2013. From univariate analyses of the onboard ChemCam calibration targets to estimates of martian rock and soil compositions. Spectrochim. Acta Part B (in press).
Forni, O., Clegg, S., Wiens, R.C., Maurice, S., Gasnault, O., 2009. Multivariate analysis of ChemCam first calibration samples. Lunar Planet. Sci. 40. Abstract #1523.
Forni, O. et al., 2013. Independent component analysis classification of laser induced breakdown spectroscopy spectra. Spectrochim. Acta Part B 86, 31–41.
Forni O. et al., 2014. First detection of fluorine on Mars: Implications for Gale crater's geochemistry. Lunar Planet. Sci. 45. Abstract #1328.
Forni O. et al., 2014. First detection of fluorine on Mars: Implications for Gale crater's geochemistry. Science (submitted for publication).
Gasnault, O. et al., 2010. Quantitative geochemical mapping of martian elemental provinces. Icarus 207, 226–247.
Gasnault O. et al., 2013. Classification of ChemCam targets from the first 100 sols in Gale crater. Lunar Planet. Sci. 44. Abstract #1994.
Gellert, R. et al., 2006. Alpha Particle X-Ray Spectrometer (APXS): Results from Gusev crater and calibration report. J. Geophys. Res. 111. http://dx.doi.org/10.1029/2005JE002555.
Gellert R. et al., 2009. The Alpha-Particle-X-ray-Spectrometer (APXS) for the Mars Science Laboratory (MSL) Rover mission. Lunar Planet. Sci. 40. Abstract #2364.
Goetz, W. et al., 2005. Indication of drier periods on Mars from the chemistry and mineralogy of atmospheric dust. Nature 436, 62–65. http://dx.doi.org/10.1038/nature03807.
Goetz, W. et al., 2010. Microscopy analysis of soils at the Phoenix landing site, Mars: Classification of soil particles and description of their optical and magnetic properties. J. Geophys. Res. 115. http://dx.doi.org/10.1029/2009JE003437.
Grotzinger, J.P. et al., 2012. Mars science laboratory mission and science investigation. Space Sci. Rev. 170, 5–56. http://dx.doi.org/10.1007/s11214-012-9892-2.
Grotzinger, J.P. et al. 2013. A habitable Fluvio-Lacustrine environment at Yellowknife Bay, Gale crater, Mars. Science (submitted for publication).
Hyvärinen, A., Karhunen, J., Oja, E., 2001. Independent Component Analysis. Wiley, New York, USA.
Johnson, J.R., Bell III, J.F., Bender, S., Blaney, D., Cloutis, E., DeFlores, L., Ehlmann, B., Gasnault, O., Gondet, B., Kinch, K., Lemmon, M., Le Mouélic, S., Maurice, S., Rice, M., Wiens, R., MSL Science Team, 2015. ChemCam passive reflectance spectroscopy of surface materials at the Curiosity Landing site, Mars. Icarus 249, 74–92.
Langevin, Y. et al., 2013. Processing approaches for optimal science exploitation of the ChemCam remote Microscopic imager (RMI) during the first 90 days of curiosity operations. Lunar Planet. Sci. 44. Abstract #1227.
Lasue, J., Wiens, R.C., Forni, O., Clegg, S.M., Maurice, S., Stepinski, T., 2011. Non-linear projection techniques for LIBS analysis: Application to ChemCam data. J. Anal. Bioanal. Chem. http://dx.doi.org/10.1007/s00216-011-4747-3.
Le Mouélic, S., Gasnault, O., Herkenhoff, K., Bridges, N., Langevin, Y., Mangold, N., Maurice, S., Wiens, R., Pinet, P., Newsom, H., Deen, R.G., Bell III, J.F., Johnson, J.R., Barraclough, B., Blaney, D., Deflores, L., Maki, J., Malin, M.C., Prez, R., Saccoccio, M., 2015. The ChemCam remote micro-imager at Gale crater: Review of the first year on Mars. Icarus 249, 93–107.
Leshin, L.A. et al., 2013. Volatile, isotope and organic analysis of martian fines with the Mars Curiosity rover. Science 341. http://dx.doi.org/10.1126/science.1238937.
Léveillé R. et al., 2013. Chemistry of fracture-filling raised ridges in Yellowknife Bay, Gale crater: Window into past aqueous activity and habitability on Mars. J. Geophys. Res. (submitted for publication).
Mangold N. et al., 2013. Chemical variations of Yellowknife Bay formation sediments analyzed by the Curiosity rover on Mars. J. Geophys. Res. (submitted for publication).
Martens, H., Naes, T., 1989. Multivariate Calibration, first ed. John Wiley & Sons, New York.
Maurice, S. et al., 2012a. The ChemCam instrument suite on the Mars Science Laboratory (MSL) Rover: Science objectives and mast unit description. Space Sci. Rev. 170, 95–166.
Maurice S. et al., 2012b. Laser Induced Breakdown Spectroscopy (LIBS) spot size at Stand-off distances with ChemCam. Lunar Planet. Sci. 43. Abstract #2899.
McGlynn, I.O., Fedo, C.M., McSween Jr., H.Y., 2012. Soil mineralogy at the Mars Exploration Rover landing sites: An assessment of the competing roles of physical sorting and chemical weathering. J. Geophys. Res. 117. http://dx.doi.org/10.1029/2011JE003861.
McSween Jr., H.Y., McGlynn, I.O., Rogers, A.D., 2010. Determining the modal mineralogy of martian soils. J. Geophys. Res. 115. http://dx.doi.org/10.1029/2010JE003582.
Melikechi, N. et al., 2013. Correcting for variable laser-target distances of LIBS measurements with ChemCam using emission lines of martian dust spectra. Spectrochim. Acta Part B (in press).
Meslin, P.Y. et al., 2013. Soil diversity and hydration as observed by ChemCam at Gale crater, Mars. Science 341.
Nachon, M. et al., 2013. Calcium sulfate veins characterized by the ChemCam instrument at gale crater, Mars. J. Geophys. Res. (submitted for publication).
Newsom, H.E. et al., 2007. Geochemistry of martian soil and bedrock in mantled and less mantled terrains with gamma ray data from Mars Odyssey. J. Geophys. Res. 112. http://dx.doi.org/10.1029/2006JE002680.
Newsom H.E. et al., 2014. Gale crater and impact processes from curiosity. Lunar Planet. Sci. 45. Abstract #1777.
Ollila, A. et al., 2013. Trace element geochemistry (Li, Ba, Sr, and Rb) using Curiosity's ChemCam: Early results for gale crater from Bradbury landing site to Rocknest. J. Geophys. Res. 119. http://dx.doi.org/10.1002/2013JE004517.
Palucis et al., 2013. Origin and evolution of the Peace Vallis fan system that drains to the Curiosity Rover landing area, Gale Crater. J. Geophys. Res. (submitted for publication).
Panne, U., Haisch, C., Clara, M., Niessner, R., 1998. Analysis of glass and glass melts during the vitrification process of fly and bottom ashes by laser-induced plasma

spectroscopy: Part I. Normalization and plasma diagnostics. Spectrochim. Acta Part B: Atom. Spectrosc. 53, 1957–1968.
Pike, W.T. et al., 2011. Quantification of the dry history of the martian soil inferred from in situ microscopy. Geophys. Res. Lett. 38, L24201. http://dx.doi.org/10.1029/2011GL049896.
Rieder, R., Wänke, H., Economou, T., Turkevich, A., 1997. Determination of the chemical composition of martian soil and rocks: The alpha proton X-ray spectrometer. J. Geophys. Res. 102, 4027–4044.
Rieder R. et al., 2004. APXS on Mars: Analyses of soils and rocks at Gusev Crater and Meridiani Planum. Lunar Planet. Sci. 35. Abstract #2172.
Sallé, B., Lacour, J.-L., Mauchien, P., 2006. Comparative study of different methodologies for quantitative rock analysis by laser-induced breakdown spectroscopy in a simulated martian atmosphere. Spectrochim. Acta Part B 61, 301–313. http://dx.doi.org/10.1016/j.sab.2006.02.003.
Sammon, J.W., 1969. A non-linear mapping for data structure analysis. IEEE Trans. Comput. C-18, 401–409.
Sautter, V. et al., 2013. Igneous mineralogy at Bradbury rise: The first ChemCam campaign. J. Geophys. Res. 119. http://dx.doi.org/10.1002/2013JE004472.
Schroeder et al., 2013. Overview of hydrogen peak signals in ChemCam Mars data. Icarus (submitted for publication).
Seber, G.A.F., 1984. Multivariate Observations. Wiley Series in Probability and Statistics.
Squyres S.W. et al., 2003. Athena Mars Rover Science Investigation. J. Geophys. Res. 108. http://dx.doi.org/10.1029/2003JE002121.
Squyres, S.W. et al., 2004. The opportunity Rover's Athena science investigation at Meridiani Planum Mars. Science 306, 1698–1702. http://dx.doi.org/10.1126/science.1106171.
Squyres, S.W. et al., 2008. Detection of silica-rich deposits on Mars. Science 23 (May), 1063–1067. http://dx.doi.org/10.1126/science.1155429.
Taylor, S.R., McLennan, S.M., 2009. Planetary Crusts: Their Composition, Origin, and Evolution. Cambridge Univ. Press, Cambridge.
Tokar, R.L. et al., 2013. Searching for chemical variation across the surface of Rocknest3 using MSL ChemCam spectra. Lunar Planet. Sci. 44. Abstract 1283.
Toulmin III, P. et al., 1977. Geochemical and mineralogical interpretation of the Viking inorganic chemical results. J. Geophys. Res. 82, 4625–4634.
Tukker, J.M., Dyar, M.D., Schaefer, M.W., Clegg, S.M., Wiens, R.C., 2010. Optimization of laser-induced breakdown spectroscopy for rapid geochemical analysis. Chem. Geol. 277, 137–148. http://dx.doi.org/10.1016/j.chemgeo.2010.07.016.
Vaniman, D. et al., 2012. Ceramic ChemCam calibration targets on Mars science laboratory. Space Sci. Rev. 170, 229–255. http://dx.doi.org/10.1007/s11214-012-9886-0.
Wänke, H., Brückner, J., Dreibus, G., Rieder, R., Ryabchikov, I., 2001. Chemical composition of rocks and soils at the pathfinder site. Space Sci. Rev. 96, 317–330.
Wentworth, C.K., 1922. A scale of grade and class terms for clastic sediments. J. Geol. 30, 377–392.
Wiens, R.C. et al., 2012. The ChemCam instrument suite on the Mars Science Laboratory (MSL) Rover: Body unit and combined system tests. Space Sci. Rev. 170, 167–227.
Wiens, R.C.S. et al., 2013. Pre-flight calibration and initial data processing for the ChemCam laser-induced breakdown spectroscopy (LIBS) instrument on the Mars science laboratory rover. Spectrochim. Acta Part B 82, 1–27. http://dx.doi.org/10.1016/j.sab.2013.02.003.
Williams, R.M. et al., 2013. Martian fluvial conglomerates at Gale crater. Science 340, 1068–1072.
Yen, A.S. et al., 2005. An integrated view of the chemistry and mineralogy of martian soils. Nature 436, 49–54.